Accepted Manuscript

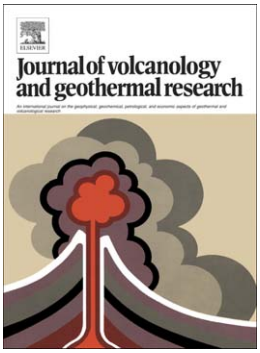

Stratigraphy of the Pleistocene, phonolitic Cão Grande Formation on Santo Antão, Cape Verde

S. Eisele, A. Freundt, S. Kutterolf, R.S. Ramalho, T. Kwasnitschka, K.L. Wang, S. Hemming

PII: S0377-0273(15)00078-5
DOI: doi: 10.1016/j.jvolgeores.2015.03.012
Reference: VOLGEO 5513

To appear in: *Journal of Volcanology and Geothermal Research*

Received date: 25 November 2014
Accepted date: 21 March 2015

Please cite this article as: Eisele, S., Freundt, A., Kutterolf, S., Ramalho, R.S., Kwasnitschka, T., Wang, K.L., Hemming, S., Stratigraphy of the Pleistocene, phonolitic Cão Grande Formation on Santo Antão, Cape Verde, *Journal of Volcanology and Geothermal Research* (2015), doi: 10.1016/j.jvolgeores.2015.03.012

Stratigraphy of the Pleistocene, phonolitic Cão Grande Formation on Santo Antão, Cape Verde

S. Eisele [a]*, A. Freundt [a], S. Kutterolf [a], R.S. Ramalho [b,c], T. Kwasnitschka [a], KL Wang [d], S Hemming [b]

[a] GEOMAR Helmholtz Centre for Ocean Research Kiel, Wischhofstr. 1-3, 24148 Kiel, Germany

[b] School of Earth Sciences, University of Bristol, Wills Memorial Building, Queen's Road, Bristol, BS8 1RJ, UK

[c] Lamont-Doherty Earth Observatory at Columbia University, Comer Geochemistry Building, 61 Route 9W/PO Box 1000, Palisades, NY 10964-8000, USA

[d] Institute of Earth Sciences, Academia Sinica, 128, Sec. 2, Academia Road, Nangang, Taipei 11529, Taiwan

* Corresponding author. E-Mail address: seisele@geomar.de

Tel.: +49 431 600 2563.

Abstract

The Cão Grande Formation (CGF) on the western plateau of Santo Antão Island is part of the younger volcanic sequence that originated from both, basanitic and nephelinitic magmatic suites, respectively called COVA and COROA suites. Based on our detailed revised stratigraphy of the CGF, including two yet unknown tephra units, we can show that both suites produced multiple, highly differentiated eruptions over a contemporaneous period. Correlations of CGF tephras with marine ash layers provide distal dispersal data for Cão Grande I (CG I) and also identify two highly explosive, phonolitic eruptions that pre-date the

CGF tephra deposits known on land. Within the CGF, the lowermost, 220±7 ka old unit Canudo Tephra (CT; COVA suite) comprises phonolitic fall deposits and ignimbrites; it is partly eroded and overlain by debris flow deposits marking a hiatus in highly differentiated eruptions. The phonolitic CG I Tephra (COROA suite) consists of an initial major plinian fall deposit and associated ignimbrite and terminal surge deposits. This is immediately overlain by the phonolitic to phono-tephritic Cão Grande II (CG II; COVA suite), a complex succession of numerous fallout layers and density-current deposits. CG I and CG II have radiometric ages of 106±3 ka and 107±15 ka, respectively, that are identical within their error limits. The youngest CGF unit, the Furninha Tephra (FT; COROA suite), consists of three foidic-phonolitic fall deposits interbedded with proximal scoria deposits from a different vent.

The phonolitic eruptions switched to and fro between both magmatic suites, in each case with a stronger first followed by a weaker second eruption. Each eruption evolved from stable to unstable eruption columns. During their terminal phases, both magma systems also leaked evolved dome-forming lavas next to the tephras. Distal ashes increase the CG I tephra volume to ~10 km^3, about twice the previously published estimate. The tephra volume of CG II is ~3 km^3; CT and FT are too poorly exposed for volume estimation. The characteristics of the CGF tephra units outline hazard conditions that may be expected from future evolved explosive eruptions on the western plateau of Santo Antão.

1. Introduction

The Cape Verde Archipelago differs from other hotspot ocean island groups in the sense that it is quasi-stationary with respect to its melting source (Burke and Wilson, 1972; McNutt, 1988). As a consequence, the archipelago represents a site of long-lived volcanism and although there is some age progression from the eastern to both the northwestern and southwestern islands, the evolutionary stages including periods of intense volcanic activity as well as periods of reduced volcanic activity dominated by erosion strongly overlap in time

between different islands (Holm et al., 2008; Ramalho et al., 2010a,b). The dominantly mafic shield-building phase on the island of Santo Antão comprised two magmatic series, an older basanite – phonolite series (7.5 – 0.3 Ma) and a younger nephelinite – phonolite series (0.7 – 0.1 Ma), which partly coexisted (Holm et al., 2006). Phonolitic products remained rare in both series during the shield-building phase but towards the end of this phase, and in transition to the erosional stage, highly explosive eruptions emplaced the voluminous phonolitic Cão Grande Formation tephras. We have logged this tephra succession in detail in order to constrain variations in eruption style and to establish the temporal order of geochemical changes and their causative petrogenetic processes. Correlations with the marine record of ash layers from the surrounding ocean floor improve the quantification of tephra dispersal. This study therefore provides the basis to explore the changes in magmatic and volcanic processes that occur during the terminal period of shield building on a highly alkalic ocean island such as Santo Antão, contributing to our knowledge on the establishment of differentiating magma chambers and ensuing large explosive eruptions. However, here we focus on the stratigraphic and chronological details while the detailed petrogenetic processes will be discussed elsewhere.

2. Geological Setting

The Cape Verde Archipelago, 500 km off the Senegalese coast (14°40’ – 17°30’ N and 21°30’ – 25°`30 W) in the North Atlantic, consists of ten major islands, several minor islets, and a number of peripheral seamounts (Fig. 1a). It is situated on the Cape Verde Rise (CVR), the largest bathymetric swell on Earth, which is thought to have formed in response to mantle plume activity (Grevemeyer, 1999; McNutt, 1988; Montelli et al., 2004; Phipps Morgan et al., 1995) or by spreading of melt residue from the hotspot (Ramalho et al., 2010b). The westward-opening, crescent-shaped archipelago can geomorphologically be divided into two island chains, a “northern chain” comprising Santo Antão, São Vicente, Santa Luzia, and São

Nicolau, and an "eastern-to-southern chain" including Sal, Boa Vista, Maio, Santiago, Fogo, and Brava (see Fig. 1a). Volcanic activity started around the Oligocene/Miocene (Torres et al., 2002) and volcanoes rest on uplifted oceanic crust made up of Jurassic pillow lavas with mid-ocean ridge basalt (MORB) affinity, uplifted relics of which occur on Maio and Santiago (Stillman et al., 1982; Gerlach et al., 1988). However, age determinations suggest that most of the islands were formed during the last 16 Ma with a slight age progression from east to west. (Holm et al., 2008; Michell et al., 1983; Plesner et al., 2002; Torres et al., 2002; Ramalho et al., 2010a,b).

Santo Antão is the second largest island of the Cape Verde Archipelago with an area of 779 km^2 (Fig. 1a). The island was initially built by three volcanic centers, the central Ribeira das Patas volcano, the younger Cova de Paul volcano in the east, and the youngest Tope de Coroa stratovolcano on the western plateau (Tarff and Day, 2013), which forms the highest peak in the island (1979 m a.s.l.) and rests on a scarp from a flank collapse at the west coast of Santo Antão (Fig. 1b). The deeply cut topography of Santo Antão corresponds to an early post-erosional stage (Ramalho et al., 2010b). Subsequently, monogenetic scoria cones, phreatomagmatic tuff cones and lava domes were emplaced. The oldest volcanics have been dated at > 7.6 Ma, and the most recent dated eruption took place at 0.09 Ma (Plesner et al., 2002). Bebiano (1932) and Holm (2006) showed that the rock compositions on Santo Antão range from nephelinitic and basanitic to phonolitic. Holm et al. (2006) distinguished the nephelinite – phonolite COROA suite and the basanite – phonolite COVA suite; however these geochemical suites occur across the structural stratigraphic units distinguished by Tarff and Day (2013).

Plesner et al. (2002) identified the Cão Grande Formation (CGF) on the western plateau of Santo Antão and Holm et al. (2006) distinguished two phonolitic to tephri-phonolitic tephra units which they termed Cão Grande I (CG I) and Cão Grande II (CG II). Type localities and

all major outcrops of the CGF are situated on the plateau east of the Tope de Coroa. The CG I pumice fallout forms a significant widespread marker bed within the youngest volcanics on Santo Antão. Plesner et al. (2002) estimated an age between 220 ka and 170 ka for the CG I fallout deposit from its stratigraphic position with respect to $^{40}Ar/^{39}Ar$ dated rock units of Santo Antão. Holm et al. (2006) showed that CG I is geochemically related to the nephelinite – phonolite COROA series, whereas CG II is related to the basanite – phonolite COVA series. A detailed stratigraphic and petrologic study of the CG I pumice fallout deposit was carried out by Mortensen et al. (2009), estimating a sub-plinian to plinian eruption from a vent close to the Tope de Coroa, but its exact location has not yet been established. We have revisited the Cão Grande Formation and expanded the earlier stratigraphy by identifying four phonolitic tephra units as described below.

3. Methods

Our on-land tephrostratigraphic profile is based on 17 logged outcrops on the western plateau of Santo Antão (Fig. 1b). Lithological and geochemical comparisons are used to correlate subunits between outcrops. A total of 70 stratigraphically logged tephra samples were taken.

In addition to land-based fieldwork, fifteen sediment cores of up to 9 m length were taken around the northern chain of the Cape Verde Archipelago during the *R/V METEOR* cruise M80/3 (Hansteen et al., 2014) (Fig. 1a) and were used to correlate marine ash beds with on-land tephras to better constrain distribution characteristics of eruptions from Santo Antão. The cores were taken at distances of 60 to 400 km from Santo Antão and at 3350 to 4320 m water depth in areas outside landslide and turbidite depositional fans as judged from bathymetric data. Visual logging of the sediment cores identified 111 ash layers, from which glass shards were separated for geochemical microanalyses. Fifteen to thirty glass shards of each sample

were analyzed by electron microprobe. Homogeneity of the shard compositions was used as one criterion to distinguish primary from reworked ash beds.

Major and minor element glass compositions of all samples as well as selected mineral compositions were analyzed on a JEOL JXA 8200 wavelength dispersive electron microprobe (EMP) at the Helmholtz Centre for Ocean Research Kiel (GEOMAR). For samples collected on land, several pumice clasts were cleaned, crushed, sieved, and the 125 – 63 µm fraction was embedded in resin (Araldite). For glass analyses we modified the method described by Kutterolf et al. (2011) due to a significant loss of Na_2O in these highly alkaline compositions. The beam current was reduced to 3 nA with a defocused beam 5 µm wide and constant acceleration voltage of 15 kV. Additionally the measurement time for Na was decreased to 5 s to minimize the migration of Na within the sample. To compensate the effects of the lower beam current on the total amount of counts the measurement time for Si and Al was increased to 30 and 40 s respectively. All analytical settings were calibrated using international, natural and synthetic standards as described in Kutterolf et al. (2011).

Trace element glass shard compositions of selected samples were analyzed by Laser Ablation Inductively Coupled Plasma – Mass Spectrometry (LA-ICP-MS) at two laboratories in Taipei, Taiwan. The LA-ICP-MS laboratory at the Institute of Earth Science, Academia Sinica in Taipei, Taiwan is equipped with a Photon Machines Analyte G2 laser ablation system using a 193 nm ArF Excimer laser attached to a magnetic sector ThermoFinnigan Element XR ICP-MS. Spot analyses were done using a spot diameter of 15 µm with 5 ns pulse duration at energy densities of 7 J/cm^2 and 5Hz repetition rate. Following 45 seconds of blank acquisition, typical ablation times were around 75 seconds. Ion intensities were measured at in the low mass resolution mode with flat top peaks. Counts for selected isotopes ^{7}Li, ^{24}Mg, ^{27}Al, ^{31}P, ^{43}Ca, ^{45}Sc, ^{47}Ti, ^{51}V, ^{52}Cr, ^{55}Mn, ^{59}Co, ^{63}Cu, ^{66}Zn, ^{69}Ga, ^{85}Rb, ^{88}Sr, ^{89} Y, ^{90}Zr, ^{93}Nb, ^{118}Sn, ^{133}Cs, ^{137}Ba, ^{139}La, ^{140}Ce, ^{141}Pr, ^{146}Nd, ^{147}Sm, ^{153}Eu, ^{157}Gd, ^{159}Tb, ^{163}Dy, ^{165}Ho, ^{166}Er, ^{169}Tm,

^{172}Yb, ^{175}Lu, ^{178}Hf, ^{181}Ta, ^{202}Hg, ^{208}Pb, ^{232}Th, ^{238}U were collected in time-resolved mode. Integration time and run replicates were set to be 30 ms and 40 ms for all the elements, respectively. Ar and He gas flows, torch position, and focusing potentials were optimized to provide a stable ion beam and low oxide production (ThO/Th < 1–1.5 %). Typical signal intensities of ^{238}U were about 200,000 cps for NIST reference material SRM 612 that was used for calibration (Norman et al., 1996) together with the USGS BCR-2g as external reference material in conjunction with internal standardization of ^{43}Ca. Internal standardization was used to correct for matrix effects and signal drift in the ICP-MS and differences in the ablation efficiency between the sample and the reference material (Günther et al., 1999). The limit of detection (LOD) for most trace elements is in sub-ppm level, basically not more than 100 ppb; for REEs LOD is approximately 10 ppb. Precision for most elements is better than 5 % (1σ). Comparison of our measured trace element contents with those reported in the literature shows differences of < 5%, demonstrating good accuracy of the LA-ICP-MS analysis in the study. Data reduction was made using Version 4.0 of "real-time on-line" GLITTER© software (Van Achterbergh et al., 2001).

The trace elements (identical set as at the Academia Sinica) determined in the Department of Geoscience at National Taiwan University were measured by coupling a New Wave UP213 laser ablation system with the Agilent 7500s ICP-MS following the method of Zhang et al. (2010). The laser ablation was performed using a helium carrier gas to reduce the deposition of ablated material onto the sample surface, which significantly improves transport efficiency and increases the signal intensity. The spot size of ablation is 30 μm, with laser repetition rate and laser energy density of 4 Hz and of 10 J/cm^2, respectively. Before and during analyzing, USGS standard glass (NIST 610) was used as the external standard and BCR-2G and BHVO-2G were also used as secondary standards for verification of analytical results. Ca (determined by EMP) was used as the internal normalization standard. All concentrations were calculated using the GLITTER 4.0 (GEMOC) software. The analytical precision is

better than 10% for most trace elements. Repeated measurements of same samples in different laboratories revealed good replication of the trace elements.

Age data for three samples (CT, CG I, CG II) have been obtained by $^{40}Ar/^{39}Ar$ sanidine dating at Lamont Doherty Earth Observatory (LDEO) of Columbia University. The sanidines were first enriched by density separation, using a sodium polytungstate liquid with a density of 2.64 in a Heraeus Labofuge 200 centrifuge. The mineral separate was then further cleaned by hand-picking. To remove adhering glass, sanidines were leached for 5 minutes in a 5% HF solution in an ultrasonic bath, rinsed three times with deionized water and then in methanol. Samples were co-irradiated for 30 minutes with Alder Creek sanidine (1.193 Ma, Renne et al., 1998) and at the USGS TRIGA reactor in Denver. Samples were measured wrapped in Ta foil and progressively heated with a diode laser. The gasses were cleaned up by exposure to SAES GP50 getters run at 2 A, and measured in static, peak-hopping mode with an analogue multiplier on a VG5400 noble gas mass spectrometer at LDEO. Measured isotope data were corrected for background contributions based on frequent measurements of the blanks, mass discrimination based on measurements of air aliquots, and nuclear interferences based on values characteristic of this reactor (values taken from Dalrymple et al., 1981). Inverse isochron ages are based on $^{36}Ar/^{40}Ar$ vs. $^{39}Ar/^{40}Ar$ correlation lines using the best-fit regression approach. Plateau ages were defined as five or more contiguous steps corresponding to a minimum of 75% of the ^{39}Ar released and showing no statistically significant slope. Additionally, integrated ages were obtained using the total released ^{39}Ar.

4. The Cão Grande Formation

In addition to the two units, CG I and CG II, of Holm et al. (2006), we have identified two more, geochemically distinct units which are missing at the Cão Grande type locality of Mortensen et al. (2009): the older Canudo Tephra (CT) and the younger Furninha Tephra (FT). CT and FT are both composed of several layers, and epiclastic deposits or intervening

mafic pyroclastic deposits variably separate these units. While CG I and II are well represented on the western plateau, we only found three outcrops of CT (SA006, SA008 and SA018, with only SA008 exposing a succession of subunits), and a single outcrop of FT (SA003) (Fig. 1b). The composite stratigraphy presented in Fig. 2 combines tephra sequences of four major outcrops and shows all layers at their maximum observed thickness. Additionally, we identified two lava domes on the western plateau of Santo Antão. The tephri-phonolitic Monte Aranha Perna (AP) (Fig. 1b) in the central part of the plateau is a strongly eroded, 250 m high dome, that is mantled by the CG I pumice. The 150 m high phonolitic Morro de Figueira dome (MF) is located about 2.5 km northeast of the Tope de Coroa Crater and 900 m west of the Ribeira de Canudo (Ribeira de Água Nova) riverbed, the type locality of CT and CG II (Fig. 1b). The dome and its two lava flows are not mantled by any of the phonolitic fall deposits but dome material covers CG II tephra at the Ribeira de Canudo riverbed, and one of the lava flows covers CG II tephra at Cabouco de Curral de Monte Figueira riverbed (another nearby tributary of Ribeira de Água Nova).

Canudo Tephra (CT)

CT covers fluvial deposits and a subjacent scoriaceous tephra sequence. The top of CT is cut by an erosive unconformity overlain by fluvial conglomerate (RW in Figs. 2, 3a) and the uppermost CT layers may be missing. Intense erosion prior to cover by CG I is the reason why CT outcrops are rarely found on Santo Antão. The most complete profile of CT is preserved at its type locality in the upper reaches of Ribeira de Canudo (Fig. 1b). We divide CT into two subunits: CT-A comprises three well-sorted and mantle-bedded fallout deposits, and CT-B comprises three ignimbrite flow units and an interbedded thin pumice fallout deposit.

CT-A starts with a reversely graded, 1 m thick lapilli fallout deposit CT-A1. Predominantly mafic lithoclasts comprising scoria lapilli and lava fragments account for 95 vol. % at the base

and decrease to 80 vol. % upwards such that the fraction of finely vesicular white to pale gray, fine to medium pumice lapilli increases from 5 vol. % at the base to 20 vol. % in the upper 50 cm of the layer. The second fallout layer (CT-A2) of white, fine to medium pumice lapilli is massive, 30 cm thick, and lithic rich (30 vol. %), with a slightly stratified top zone capped by a 1 cm thick white, fine to medium ash bed. CT-A3 is a 75 cm thick layer of white, coarse pumice lapilli with blocks and bombs up to 20 cm in diameter and an enrichment of lithic (20 vol. %) fragments at the top.

The overlying CT-B1 is a 30 cm thick, poorly-sorted, well-cemented, white tuff with reversely coarse tail-graded coarse pumice lapilli (20 vol. %) and minor lithoclasts (10 vol.%); we interpret CT-B1 as a thin ignimbrite flow unit. CT-B2 consists of two 5 cm thick, medium-lapilli pumice fallout layers separated by a 1 cm thick ash bed.

The layers CT-B3 and -B4 are two poorly-sorted tuffs above a planar erosional unconformity cutting the CT-B2 fallout deposits. The 1.5 m thick tuff B3 has a pumice enrichment at the top. Overlying tuff B4 is ≥ 4.5 m thick. Both tuffs contain 20 vol. % lithoclasts and 30 vol. % white medium pumice lapilli in a fine ash matrix. We interpret these two tuff beds as ignimbrite flow units. The top of B4 is an erosional unconformity that is covered by fluvial deposits (RW in Figs. 2 and 3a).

Cão Grande I Tephra (CG I)

CG I is a bipartite unit comprising an up to 8.5 m thick, well-sorted, white to pale gray pumice lapilli fallout deposit CG I-A, which mantles the topography, and an up to 2 m thick subunit CG I-B composed of several flow deposits. CG I is best preserved on the western plateau of Santo Antão but forms a significant marker bed on the rest of the island. Mortensen et al. (2009) noted lithological and geochemical changes across the CG I fallout but did not stratigraphically subdivide the deposit. Here we identify subunit CG I-A1 that is composed of

two main massive fallout layers of angular, phenocryst-poor, medium to coarse pumice lapilli. The two layers are separated by a 5 cm thick horizon of fine pumice lapilli that occurs 4.5 m above the base at the type locality. The basal 20 cm of the fallout are enriched in angular mafic lithoclasts (20 vol. %). In the upper 1.75 m the abundance of phenocrysts increases to 5 vol. % and cumulates of sanidine, haüyne and amphibole within the pumice clasts are common. The uppermost meter of CG I-A1 is slightly stratified and the content of accidental mafic lava fragments increases from 1-2 vol. % to 80 vol. % at the top (Fig. 3c). Overlying CG I-A2 comprises several 30-40 cm thick, poorly-sorted, lithic-rich, massive fine ash to coarse pumice lapilli flow deposits that were deposited towards the northern flank of the island.

Subunit CG I-B is divided into a lower 50 cm thick, lithic-rich, stratified layer (CG I-B1) with a 15 cm alternating fine to coarse basal ash and a 35 cm thick top with alternating medium ash and fine to medium lapilli beds. It contains up to 80 vol. % lithics ranging in size from fine ash to 20 cm blocks. These blocks have been emplaced as ballistic impacts as evident from deformation of underlying beds. Layer B1 is proximally cut sharply by an unconformity on which lies the basal tuff of CG I-B2, an accretionary lapilli bearing, 1.1 m thick sequence of alternating fine to coarse ash beds. The amount of lithics is similar to CG I-B1 but grain sizes up to coarse lapilli are significantly smaller. Cross-bedding and antidune structures are common in both layers of CG I-B (Fig. 3c), which supports our interpretation as surge deposits.

Cão Grande II Tephra (CG II)

Based on changes in lithological and geochemical compositions, we distinguish five major subunits in CG II (CG II-A-E), each comprising several layers. The lowermost layer CG II-A1 is a 20-60 cm thick pinching and swelling deposit that is planar and cross-bedded and overlies a basal unconformity that cuts into the topmost CG I-B deposits (Figs. 2, 3c). Layer

A1 contains lenses and horizons of angular, moderately vesicular, fine pumice lapilli, interbedded with fine to coarse ash layers that form dune-like structures. We therefore interpret that layer A1 was emplaced by pyroclastic surges that marked the beginning of CG II eruptions. The CG II-A1 surge deposits are capped by a 10 cm thick well-sorted fallout layer of gray, medium to fine pumice lapilli (CG II-A2) which is in turn overlain by a second, thinner surge deposit.

Subunit CG II-B is a 4 m thick succession of nine well-sorted lapilli fallout layers and three tuff layers (CG II-B1-12). The lithic-poor (0-10 vol. %) fallout layers are composed of beige and pale-gray to gray, highly vesicular, fine to coarse pumice lapilli. Layers B1, B2, and B3 are moderately well sorted with an increased fraction of fine lapilli and coarse ash compared to the other fallout deposits of CG II-B. The gray B2 tephra in addition is symmetrically reverse to normal graded and grain sizes up to medium lapilli are significantly smaller compared to B1 and B3. Layers B5, B6, B7, B8 and B9 are well sorted and ash-free lapilli beds. B5 is inversely graded from medium to coarse lapilli, whereas B6 through B9 are massive. Coarse lapilli layers B6 and B9 are the coarsest beds, whereas B7 and B8 are composed of medium lapilli. The two prominent gray lapilli layers (CG II-B2 and -B8), as well as two thin fine to coarse ash layers (CG II B4 and B10) are useful marker beds in the fallout sequence. A 10 cm thick gray medium ash layer (CG II-B12) marks the top of subunit B.

Subunit CG II-C has higher contents of lithics (25-30 vol. %) and phenocrysts (20 – 40 vol. %) compared to CG II-B, and is sub-divided into five layers (CG II-C1-5). CG II-C1 is a 20 cm thick, mantle bedding, moderately-sorted, lithic-rich (30 vol. %) fallout layer, that contains gray, medium pumice lapilli, and has a 10 cm thick, cemented, massive, gray, coarse to medium ash tuff on top (CG II-C2). CG II-C3 is 35 cm thick and composed of well-sorted, crystal rich (40 vol. %), normally graded dark gray coarse to fine ash with low-angle cross-

bedding indicative of a pyroclastic surge. The overlying 15 cm of moderately-sorted, yellowish to gray, fine to medium pumice lapilli form fallout bed CG II-C4. Layer CG II-C5 is a pyroclastic surge deposit that pinches and swells from 35 to 50 cm in wavy fashion and is composed of individually well-sorted, multiple normal-graded dark gray coarse to medium ash layers similar to layer C3. The wavy top of CG II-C is cemented and not eroded.

Subunit CG II-D mantles the surface topography of the CG II-C deposits and is composed of a 35 cm thick, well-sorted, inversely graded, beige medium pumice lapilli layer (CG II-D1) which gradually changes into a 40 cm thick poorly-sorted massive tuff (CG II-D2). It is overlain by a >20 cm thick, well-sorted, lapilli fallout (CG II-D3) containing white coarse pumices and bombs up to 50 cm in diameter. CG II-D4 is a 35 cm thick, poorly-sorted massive tuff with fine to medium pumice lapilli, which we interpret as an ignimbrite overbank facies.

The CG II profile at the type locality terminates with a 1.6 m thick sequence of nine alternating fine to coarse ash and fine to medium pumice lapilli fallout layers. CG II-E1 is a 15 cm thick, slightly cemented, well-sorted, gray fine to medium ash, capped by a 10 cm thick light gray medium lapilli pumice fallout deposit (CG II-E2). CG II-E3 is a 65 cm thick, poorly-sorted, reddish-gray lapilli tuff comprising medium pumice lapilli, 50 vol. % of lithoclasts and a fine to coarse ash matrix. We interpret CG II-E3 as a pyroclastic flow deposit. The following 85 cm thick sequence is composed of three 10 cm thick, well-sorted, gray pumice fine to medium lapilli fallout layers alternating with dark gray massive tuff beds (CG II-E4-9) totaling 55 cm in thickness.

Furninha Tephra (FT)

In the Furninha Laie riverbed, a crosscut of the Cão Grande riverbed (Fig. 1b), the thick mafic scoria lapilli deposits of a nearby scoria cone are interbedded with three phonolitic pumice

lapilli fallout deposits which we group as the Furninha Tephra (Fig. 2). Apart from the intercalated phonolitic beds, the exposed scoria succession does not show evidence for significant breaks in mafic eruptions such as paleosols or major unconformities. Layer FT-A1 is a 15 cm thick, massive, well-sorted fallout deposit consisting of gray medium pumice lapilli. A 9 m thick sequence of alternating fine to coarse scoria lapilli layers separates this from FT-A2, a 15cm thick moderately well-sorted lapilli layer of gray medium pumice clasts. This is concordantly overlain by the 50 cm thick FT-A3 tephra that is compositionally zoned from pale gray pumice lapilli at the base to black scoria lapilli at the top (Fig. 3b), with mixed pumiceous clasts in the middle part. This unit most probably represents the latest known explosive stage of the phonolitic Cão Grande magma system.

5. Compositional variations

5.1 Compositional differences between units

Based on the total alkali versus silica diagram (Le Maitre et al., 1989), the whole-rock compositions of CT and CG I are classified as phonolites each forming a discrete field, with CG I exhibiting higher alkali contents (Fig. 4). Pumices extracted from Unit CG II range from tephri-phonolite composition in subunit CG II-A through phonolite in CG II-B pumice to tephri-phonolite to phono-tephrite in CG II-C-E. Unit FT pumice is foidic-phonolite (ca. 50 wt. % SiO_2) and the scoriaceous top of FT-A3 has the least evolved composition (ca. 45 wt. % SiO_2) of the entire Cão Grande Formation. The Monte Aranha Perna and Morro de Figueira lava domes are tephri-phonolitic and phonolitic, respectively.

Holm et al. (2006) recognized two magmatic series on Santo Antão both extending towards phonolitic compositions. They showed that CG I is associated to a nephelinite-trend (COROA trend) characterized by high Zr contents, whereas CG II belongs to the basanite-trend (COVA trend) with lower Zr contents (Fig. 5). According to this classification, CT represents the

evolved end member of the basanite-trend. The AP dome also corresponds to this trend and overlaps with CG II compositions. FT and the MF dome are associated with the nephelinite-trend (Fig. 5).

5.2 Compositional variations within units

The mineral content and assemblage in pumice clasts of the Cão Grande Formation can be used as a tool to distinguish and correlate single subunits. Visual observations on hand specimen are supported by calculated mineral contents of representative samples (see supplementary data) using the mixing software in IgPet 2010 (Carr, 2000). The major element mass balance calculations determine the amount and composition of the mineral assemblage required to derive the analyzed glass composition from the bulk-rock composition, using analyzed phenocryst compositions; only results with sum of least-squared residuals <0.1 were accepted. The calculated mineral contents are in general higher than the visual estimations (Fig. 6; Tab. 1) but relative changes within the stratigraphic order are identical with both methods.

Canudo Tephra

The samples of CT are all very similar except of CT-A1. They are generally characterized by a mineral content of around 25 vol. % dominated by sanidine and plagioclase with minor haüyne, clinopyroxene, amphibole and rare FeTi-oxides, sphene and apatite. The microvesicular CT-A1 differs from the other CT samples by its microlite-rich matrix dominated by sanidine and plagioclase crystals, whereas the phenocryst species are similar. Felsic cumulate fragments composed of plagioclase, sanidine and haüyne occur throughout the entire sequence of CT, whereas mafic cumulates dominated by amphibole and clinopyroxene with minor sphene and FeTi-oxides are only observed in the ignimbrite flow units CT-B3 and B4.

Cão Grande I Tephra

For CG I we were unable to calculate the crystal contents as bulk rock and glass compositions are close to each other and to sanidine compositions, which is the predominant phenocryst phase. Macroscopic and microscopic observations yield estimated mineral contents of ≤ 1 vol. %, in agreement with Mortensen et al. (2009). The surge deposits of CG I-B tend to have slightly higher mineral contents (< 5 vol. %), but the mineral assemblage is similar to CG I-A. The assemblage is strongly dominated by sanidine with minor clinopyroxene, FeTi-oxides, haüyne, amphibole, sphene and rare apatite and plagioclase. As in CT two types of cumulates occur within the CG I pumice clasts. A felsic cumulate consisting of sanidine and haüyne, and a mafic cumulate made of clinopyroxene, amphibole and FeTi-oxides with minor apatite and sphene. The mafic cumulates are increasingly abundant towards the top of CG I-A1. Despite the very low phenocryst contents an upward increase of mafic phenocrysts can be observed in the CG I fall deposit.

Cão Grande II Tephra

Subunits CG II-A and B are characterized by intermediate phenocryst contents (~35 vol. %) with predominant sanidine, minor amphibole, plagioclase, clinopyroxene, haüyne and rare FeTi-oxides, sphene and apatite. With the transition from CG II-B to CG II-C the mineral contents of pumice clasts increase to ~50 vol. %. The mineral assemblage, in comparison to CG II-A and –B, is no longer dominated by only sanidine but 70-80 vol. % of the assemblage are composed of sanidine, plagioclase and amphibole in approximately equal proportions. The contents of clinopyroxene, Fe-Ti-oxides and sphene are also slightly increased but still minor compared to CG II-A and -B. Apatite still occurs rarely but haüyne is missing in CG II-C.

Furninha Tephra

The phenocryst assemblage of FT-A1 pumice (ca. 45 vol.%) is mostly composed of sanidine, clinopyroxene and haüyne with minor magnetite, sphene and amphibole and rare apatite. The phenocryst contents of pumice in FT-A2 and the lower part of the compositionally zoned FT-A3 are significantly lower (ca. 30 vol. %) and the assemblages are strongly dominated by clinopyroxene with common amphibole, haüyne and sanidine and minor magnetite, sphene and apatite. The scoria in the upper part of the compositionally zoned FT-A3 has high phenocryst contents (ca. 50 vol. %) with predominant clinopyroxene and amphibole and minor feldspars. The minor magnetite and sphene contents in the scoria are higher than in FT-A3 pumice, but haüyne is absent.

6. Ages of the Cão Grande Formation

Table 2 lists the new $^{40}Ar/^{39}Ar$ age data we have determined for CT-B3, CG I-A1 and CG II-D3 (detailed isotope data is presented in the supplement). Inverse isochron, plateau and integrated ages for each sample overlap largely within their error limits (Tab. 2); for simplicity, we only refer to the inverse isochron ages in the text. The ages obtained for the specific stratigraphic samples represent the age for the entire stratigraphic unit since no significant time gaps between single subunits are indicated. We obtained an age of 220 ±7 ka for the CT eruption that implies a considerable time gap to ages of 106±3 ka for CG I and 107 ±15 ka for CG II. These practically identical ages of CG I and CG II agree with the geological observation of direct contact of primary CG I and CG II deposits without intervening epiclastic deposits or weathering horizon. The unconformity and fluvial deposits separating CT and CG I, on the other hand, represent an ~100 ka volcanic hiatus.

Plesner et al. (2002) did not date CGF tephras themselves but bracketed the CG I age to 220-170 ka, using the age of underlying lavas and the age of Tope de Coroa volcano, respectively. However, no geological evidence is provided to demonstrate that the dated lavas from Tope de Coroa volcano are indeed younger than CG I. Our dating results show that CG I is ~60 ka

younger than the 170 ka age, although there are some deposits of Tope de Coroa volcano that indeed overlie CG II (see Fig. 3a), implying that Tope de Coroa has a long eruptive history covering many ten thousand years.

7. Correlation to marine tephra record

In the northern chain of the Cape Verde Archipelago, Santo Antão is the only island known to have produced large explosive eruptions during the last 300 ka (Plesner et al., 2002; Duprat et al., 2007; Jørgensen and Holm, 2002). The pumice deposits of the CGF represent the largest known explosive eruptions on Santo Antão, by far, within this time period. In the 15 cores collected around the northern island chain (Fig. 1a; detailed core descriptions are listed in the supplement A), 12 mafic and 15 felsic ash beds (Fig. 7) have homogeneous glass-shard compositions and appear to be primary tephra layers distinct from reworked ash layers which we identify by heterogeneous glass-shard compositions. In this study we will concentrate on the felsic ash layers. Of the 15 felsic ash beds, 14 are massive but one shows cross-bedding structures possibly from vertical density plumes impinging on the seafloor (cf. Carey, 1997). However there is a continuous spectrum of admixed bioclasts and other clastic sediments as well as of stratification textures. Moreover ash beds of identical homogeneous glass compositions occur multiply in one core. Therefore some of these ash beds must be reworked despite their homogeneous glass composition and although clear lithological and structural evidence for secondary emplacement is absent.

Each pumice unit of the CGF defines a distinct compositional field in major and trace element variation diagrams (Fig. 8), which can be used for correlations with marine ash layers. In terms of major element compositions all 15 felsic ash beds are phonolites similar to the CGF (Fig. 8a), but only four of the layers have trace element compositions compatible with the particular CGF unit (Fig. 8b). In detail, the marine ash layers in cores M80/3-1383 (234-243 cm below seafloor = cm bsf) and M80/3-1384 (345-355 cm bsf) can be correlated to unit CG I.

Core M80/3-1384 contains another ash layer (340-341 cm bsf; Fig. 7) that has similar major element compositions as the underlying ash layer (345-355 cm bsf) (Fig. 8a), but differs by its lower amount of pumice glass shards and is interpreted as reworked CG I material. Ash beds in cores M80/3-12 (461-463 cm bsf) and M80/3-91 (243-259 cm bsf, 274-284 cm bsf, 356-360.5 cm bsf) also show a similar major element composition as CG I (Fig. 8a), but differ significantly in trace elements (Fig. 8b); these ash beds represent eruptions not yet recognized on land. Marine ash layers in cores M80/3-78 (263-267 cm bsf) and M80/3-93 (402 cm bsf) correlate to CG II by their major and trace element compositions. Tephras in cores M80/3-80 (210.5 cm bsf, 219-221 cm bsf, 463-471 cm bsf), M80/3-89 (98-102 cm bsf, 291-293 cm bsf) and M80/3-93 (90 cm bsf) also have CG II major element compositions but trace element data are not available. Multiple occurrences of CG II layers in the cores (Fig. 7) clearly show that not all of them can be of primary origin.

CT ash beds were not found in the marine cores, probably because of insufficient penetration depths. As suspected from the small thicknesses and the limited dispersal on land, ash beds from FT are not present in any of the marine cores.

8. Discussion

8.1 Facies interpretation of the Cão Grande Formation

Canudo Tephra

The CT eruption initiated with a conduit-clearing explosion, producing a massive lithic lapilli fallout deposit (CT-A1), with initially only a few percent magma erupting. However, the juvenile fraction increases from A1 through A3 at the expense of the lithic fraction, suggesting stabilization of the conduit leading to the steady eruption conditions that formed the massive pumice fallout A3. The increase in grain size from A1 to A3 reflects the increased mass eruption rate that was facilitated by erosive vent widening. This build-up was

not continuous as evident by the thin ash bed on top of A2, which suggests a short weakening of the eruption.

We interpret CT-B as a phase of unstable eruption conditions when several pyroclastic flow-units were formed by eruption column collapses. A temporary recovery to a stable eruption column formed fallout B2. A lithic enrichment at the top of fallout A3, and the general return to higher lithic contents in the CT-B tuffs, suggests further widening of the conduit such that the consequently increased mass flux most probably exceeded the critical value for stable column conditions (e.g., Woods, 1988). We see no evidence for other factors that may have affected eruption stability such as decreased volatile release (reduced pumice porosity) or influx of external water (e.g., abundant ash aggregates).

Cão Grande I Tephra

According to Mortensen et al. (2009), the lithic-rich, slightly stratified basal part of CG I-A1 represents the vent clearing phase of the CG I eruption followed by the main pumice lapilli deposit formed from a sustained sub-plinian to plinian eruption column. Mortensen et al. (2009) interpreted the increasing abundance of lithics in the upper 2 m of the CG I-A1 fallout deposit as the result of gradual collapse of the volcanic conduit. They also described CG I-A2 as block and ash flows but did not go into further detail.

We interpret CG I-A2 as proximal pyroclastic density currents formed by collapses of the eruption column. Such collapse may have been caused by mass flux increased by vent widening (e.g., Woods, 1988) and/or by cooling of the erupted mixture by the abundant entrained lithics (e.g., Koyaguchi and Woods, 1996).

Considering the abundance of accretionary lapilli in proximal and medial outcrops as well as low angle cross-bedding and antidune structures of poorly sorted, lithic-rich material in proximal deposits of the conformably overlying CG I-B (Fig. 3c), we interpret these tuff

deposits as pyroclastic surge deposits generated during phreatomagmatic explosions. The upward-increasing, high abundance of accretionary lapilli in CG I-B - some being composed of coarse ash - seems more compatible with abundant influx of water at the vent rather than simple condensation of moisture in the eruption column. As there is no evidence (in the form of lacustrine sediments below CG I or indeed anywhere in the Cão Grande Formation sequence) for the existence of a surface lake on the western plateau, we infer that invasion of ground water into the conduit possibly facilitated by decreasing eruption rate was the cause of the phreatomagmatic terminal activity of CG I.

The tuff deposits corresponding to our units CG I-B and CG II-A1 (interval marked by * in Fig. 2, Fig. 3c) have been interpreted as mudflow deposits separating CG I and CG II by Mortensen et al. (2009). We have interpreted these deposits as primary pyroclastic surge deposits formed by phreatomagmatic explosions. This interpretation based on lithological compositions and structures is supported by geochemical compositions which show that the lower surge beds (CG I-B1 and –B2; Fig. 3c) are associated to CG I while the upper beds (CG II-A1; Fig. 3c) represent the initial phase of CG II; i.e., the immediate contact between primary CG I and CG II deposits lies within this tuff package. Our interpretation is supported by the practically identical radiometric ages of CG I and CG II.

Cão Grande II Tephra

As mentioned above the CG II eruption began with violent explosions that emplaced the lithic-rich, poorly-sorted, low angle cross-bedded pyroclastic surge deposits of CG II-A (Fig. 3c). The fine-grained deposits have wet-surge characteristics (e.g., Valentine and Fisher, 2000) and we interpret that the explosions were of phreatomagmatic origin. The juvenile pumice, however, is highly vesicular such that magma-water interaction must have occurred well above vesiculation depths within the vent. The 10 cm thick fine pumice lapilli fallout

intercalated between the surge deposits represents a short period when a high eruption column was attained.

Stable magmatic eruption conditions allowed the formation of sustained eruption columns during the eight successive events that formed pumice fallouts CG II-B1-3 and CG II-B5-9. The minor lithological changes between the CG II-B layers reflect the different intensities of the eruptive phases. The interbedded thin lithic-rich, poorly-sorted ash deposit (CG II-B-4) suggests a short-term return to magma-water interaction. The alternating thin well-sorted ash and fine lapilli fallouts at the top of CG II-B formed by variably weak, short eruption pulses.

During subsequent formation of CG II-C, unstable collapsing eruption columns produced the pyroclastic surges that emplaced thick gray, slightly planar stratified to low angle cross-bedded, ash deposits interbedded by thin moderately-sorted lapilli layers. The surge deposits are relatively well-sorted and lack fine ash, characteristics that suggest relatively dry transport conditions (e.g., Valentine and Fisher, 2000); therefore this eruption phase was probably not associated with a return to magma-water interaction.

The two massive, mantle-bedding fall deposits (CG II-D1 and -D3) show that the eruption had recovered to temporarily stable conditions although each event terminated with column collapse emplacing a pyroclastic flow deposit atop each fallout (CG II-D2 and -D4). In the absence of any evidence for dramatic changes in wind direction, the increase in grain size from C to D lapilli layers suggests an increase in mass eruption rate and we interpret that column collapses occurred because critical mass eruption rates were exceeded.

The significant decrease of grain size and layer thicknesses in subunit CG II-E (alternating well-sorted ash and thin lapilli beds) shows dramatically weaker eruptive activity during the terminal phase of CG II. This included emplacement of the thick, massive, poorly-sorted tuff (CG II-E3) by a pyroclastic density current. We speculate that the flow originated from a

collapsing eruption column but cannot exclude the possibility that interaction of magma with water occurred as indicated by a high lithic content (50 vol. %).

Furninha Tephra

The intercalation of subunit FT pumice fallouts within the scoria cone deposits suggests the coexistence of two volcanic systems with very different compositions erupting over the same time period. In the absence of further outcrops, the three FT pumice fallout layers cannot be put into a context of eruption processes. The scoria succession between layers A1 and A2 suggests some time break in FT activity while the concordant succession of layers A2 and A3 may reflect two rapidly following erupting pulses; however, there may also have been a break in activity at the scoria cone at that time. The compositional zonation (Fig. 3b) and magma mingling structures of FT-A3 offer the possibility that the FT pumice eruptions may have been triggered by intrusion of mafic magma into a phonolitic reservoir. Whether or not this mafic magma was related to the scoria cone eruptions requires further analyses.

Phonolitic domes

The Monte Aranha Perna dome is compositionally associated to the basanite-phonolite COVA trend (Fig. 5) and therefore could be genetically related to CT or CG II. Its top is covered by pumice of the CG I fall deposit, and therefore its extrusion during the CG II eruption can be ruled out. Without any age constraints there is no field evidence for a connection of Monte Aranha Perna dome to CT, so speculations about such association rely on geochemical similarity only. The possibility remains that the dome just represents an independent phonolitic event older than CG I at the western plateau of Santo Antão.

The younger Morro de Figueira dome is related to the nephelinite – phonolite COROA trend (Fig. 5) and by its stratigraphic position above CG II we interpret the Morro de Figueira to be the latest phonolitic unit on Santo Antão. This is consistent with its youthful, virtually

uneroded morphology. It may be genetically related to FT as a more evolved component of that magma system, or it may represent a distinct event. Possible petrogenetic relations between the domes and the CGF tephras will be further discussed in a forthcoming paper focusing on the geochemistry of the CGF.

8.2 Marine tephrostratigraphy of the CGF

No ash traces of CT and FT compositions have been found in the M80/3 gravity cores (Fig. 7). The following discussion thus focuses on CG I and CG II.

Cão Grande I Tephra

We have found CG I ash beds in cores M80/3-1384 and -1383 some 300-400 km ENE of Santo Antão (Fig. 1a). In core M80/3-1384 we found CG I ash traces at 340-341 cm bsf and 345-355 cm bsf (Fig. 7). Due to its lower amount of glass shards and lower thickness we interpret the upper of these two ash beds as reworked CG I material, though there is no structural and textural evidence for reworking. Core site M80/3-1384 is located 25 km away from Senghor Seamount and 40 km away from Sal (Fig. 1a), and both have steep submarine slopes towards site M80/3-1384 (~ 5 % at Sal, ~11% at Senghor Seamount). We therefore conclude that this upper reworked ash bed represents distal runout of slumping of ash from these slopes. Conversely, ash beds M80/3-1384, 345-355 cm and M80/3-1383, 234-243 cm represent primary distal deposits of CG I. The pelagic sediment thicknesses above the primary, 106 ka old CG I ash beds suggest average sedimentation rates of 2.2 to 3.3 cm/kyr at sites 1383 and 1384.

The absence of CG I in all cores but M80/3-1383 and -1384 (Fig. 1a) suggests a narrow dispersal fan towards the ENE. However, cores M80/3-88, -89, -93, -92 and -91, that are located between M80/3-1384 and Santo Antão, also do not contain CG I ash (Figs. 7, 9a). In the case of core sites close to the island chain (M80/3-88, -89, -93 and -92) this deficit can be

explained by high sedimentation rates in combination with relatively short core lengths (2.5-6 m), so that the depth of the CG I tephra was simply not reached. However, ash of CG I is also absent in the 8.79 m long core M80/3-91 (Figs. 7, 8, 9a). The above explanation for the other core sites may not apply here because CG II ash beds are also missing in core M80/3-91. Rather than invoking a sediment succession that is too young, we here interpret that the sediment succession is too old and that CG I and younger materials are absent due to submarine erosion. Although no erosional unconformity is visible in the core, this interpretation is supported by the presence of non-CGF phonolitic ash beds in core M80/3-91 that are absent in the neighboring shorter cores. Moreover, if M80/3-91 sediments were all younger than CG I this would imply an average sedimentation rate of >8 cm/kyr that is unusually high compared to our above estimates of 2.2-3.3 6 cm/kyr for sites 1383 and 1384 and to 1.9-2.6 cm/kyr obtained for the Cape Verde Rise by Eisma and Passchier (1978).

A ENE dispersal of CG I fallout would agree with the data of Mortensen et al. (2009) who estimated eruption column heights around 30 to 34 km from isopleth data using the method of Pyle (1989). However, for such column heights, the present annular vertical wind profile over the Cape Verdes based on monthly averages between 1968 and 1996 (NOAA-CIRES, 2001) would predict a westward dispersal of the ash if the general wind pattern 106 ka ago had been the same as today. With this prerequisite, the observed eastward distribution of the CG I fallout (Fig. 9a) could be explained by lower eruption column heights between 21 and 26 km. Numerical models of Graf et al. (1999) and Herzog et al. (1998) suggest that the modeling applied to the isopleth data (Pyle, 1989) possibly overestimated column heights by neglecting effects of adiabatic cooling and of crosswinds on the plume. We therefore suggest a lower eruption column height of 21 to 26 km for the subplinian to plinian CG I eruption and a dispersal to the east in agreement with the current wind directions at this stratospheric height.

Cão Grande II Tephra

Marine ash beds correlated to CG II are identified in several cores located in a half circle north of Santo Antão with a distance of 90 to 145 km from the western plateau (M80/3-78, -80, -89 and -93, Fig.1a). These ash beds are composed of compositionally homogeneous glass shards (Fig. 8a) and are mostly massive but some are cross-bedded. They show no erosional contacts to underlying sediments, or other clear evidence of reworking (see supplement A). Yet none of them can be clearly identified as a primary ash fallout layer of CG II. One reason for this is that their stratigraphic position in the core is too young (e.g. M80/3-93, 402 cm bsf) as evidenced by the occurrence of older, heterogeneous, reworked beds that contain CG II ash mixed with CG I and other, more mafic glass-shards (e.g. M80/3-93, 501-503 cm bsf) (Fig. 7). Another reason is that the amount of homogeneous vitric ash is low compared to the content of admixed mussel and foraminifera fragments, which indicate extensive lateral transport along the seafloor (e.g. M80/3-78, -80 and -89). Additionally, cross-bedded, geochemically heterogeneous tephra beds are abundant in the cores M80/3-57, -78, -80, -87, -88, -89 and 93 (supplement A) suggesting that secondary lateral transport of sediments was very common at these locations. We therefore interpret these tephra beds as reworked ash layers associated to slumping of slope sediments and/or primary ash beds. Considering the immediate concordant contact between CG I and CG II on land, and their near-identical radiometric ages, we would expect to find primary marine CG II ash close above marine CG I ash. Since the gravity cores (M80/3-78, -80, -87, -88, -89, -92, and -93) did not reach CG I, they most likely also did not reach primary CG II layers, due to high sedimentation rates caused by slumping and high sediment input from the island flanks. On the other hand, we did not find CG II ash above the CG I ash in the distal cores (e.g. M80/3-1383 and -1384) although the areal distribution of CG II on the western plateau of Santo Antão also indicates eastward dispersal. We therefore conclude that the CG II eruption was weaker than the earlier CG I eruption.

Non-CGF ash layers

Cores M80/3-91 and -12 (Fig. 7) contain ash layers that are similar to the CG I ash in major element glass compositions (Fig. 8a) but clearly differ in trace elements (Fig. 8b). We therefore conclude that these phonolitic ash layers are not part of the CGF as defined on land. M80/3-91 contains three of such ash layers at 243-259 cm bsf, 274-284 cm bsf and at 356-360.5 cm bsf, which are all similar in major and trace element glass compositions (Fig. 8). None of these layers shows clear evidence for lateral transport due to reworking (see supplement A). However, the glass shards content decreases from the lowermost bed (356-360.5 cm bsf) to the uppermost bed (243-259 cm bsf). We therefore interpret that the upper two beds (243-259 cm bsf and 274-284 cm bsf) consist of reworked material and only the lowermost layer is a primary fallout deposit. We cannot, however, completely exclude the alternative interpretation that the three layers represent three eruptions that discharged magma of equal composition (but separated by 6 and 32 kyr pauses estimated from a typical pelagic sedimentation rate of 2.2 cm/kyr). Apart from Santo Antão, phonolites are also known from São Vicente and São Nicolau islands in the northern chain (Fig. 1a; Jørgensen and Holm, 2002; Ancochea et al., 2010; Duprat et al., 2007). However, these phonolites are much too old to be correlated to our marine ash beds. Trace element ratios of the M80/3-91 phonolitic ash beds are similar to those of phonolite from the Proto Coroa group on Santo Antão (Holm et al., 2006) (Fig. 8b) and we therefore speculate that the non-CGF ash beds may represent evolved explosive eruptions during the Proto Coroa period. This interpretation fits with our aforementioned argumentation that core M80/3-91 is older than the neighboring cores.

The ash in core M80/3-12 (461-463 cm bsf; Figs. 1a, 7, 8) has a different trace element composition and we do not know any potentially correlative compositional equivalent from land.

8.3 Tephra volumes

The best method to estimate the volume of fallout deposits is to integrate linear regressions through data on ln [isopach thickness] versus square root [isopach area] plots following Pyle (1989) and Fierstein and Nathenson (1992), provided sufficient proximal, medial and distal outcrops are available. We use our marine tephra data for CGF tephras to complement the tephra volume estimation of Mortensen et al. (2009) that was just based on proximal data of CG I. For this estimation we assume that the core locations of M80/3-1383 and -1384 (Fig. 1a) lie on the fan axis and the measured tephra thickness represents the maximum thickness at this distance. The distal isopachs for CG I are shown in Fig. 9a. The new minimum tephra volume is 10.33 km^3 (VEI 6) for CG I (Tab. 3) which does not include the volume of the CG I flow deposits which must be relatively small considering the small number of outcrops confined to narrow channels. To convert the tephra volume into a dense rock equivalent (DRE) magma volume we reduced the proximal to medial volume by 50% to account for the pore space and lithic content, and the distal volume by 30%, respectively; these values have been empirically estimated from a large number of tephras by Kutterolf et al. (2008). The resulting DRE volume of 5.6 km^3 (Tab. 3) is twice the value estimated by Mortensen et al. (2009). The corresponding erupted magma mass is 13.5 $x10^{12}$ kg (magnitude 6.1).

No reliable isopach map can be constructed for CG II because most outcrops on land are eroded at the top and the marine gravity cores did not reach primary ash fallout layers. In order to obtain an approximate minimum tephra volume of CG II, we summed up the thicknesses of the ash layers containing CG II shards in each core, and then subtracted 10-85% for lithoclasts and entrained marine sediments, and 0-80% for admixed glass shards from other eruptions, where the respective percentages have been estimated from smear slides and EMP analyses. Based on these data, the 8 cm and 4 cm isopachs were drawn (Fig. 9b). In addition, we assumed an average thickness of 1.5 m for CG II deposits on land. The resulting CG II minimum tephra volume then becomes ~3 km^3 (VEI 5). Applying the corrections for pore space and lithic content after (Kutterolf et al., 2008) as for CG I above, the DRE magma

volume becomes 1.1 km^3, corresponding to 2.7 $x10^{12}$ kg erupted magma mass (magnitude 5.4) (Tab. 3).

Tephra volumes of CT and FT cannot be estimated from the very small number of preserved outcrops.

8.4 Temporal evolution of CGF

Our new $^{40}Ar/^{39}Ar$ sanidine ages for CT, CG I and CG II provide the first direct dating of the CGF. In agreement with field observations, which show an erosional unconformity and intercalated debris deposits, we now quantify a time break of ~100 kyrs between CT and CG I, whereas the concordant direct contact between CG I and CG II and their statistically identical radiometric ages do not allow for any significant time break between these two large eruptions. The age of the FT eruption remains unknown but a time break in the eruption history of the CGF is clearly shown by the eroded top of CG II (exposed at its type-locality), as well as a thin soil at the transition from CG II to the overlying scoria cone deposits.

Mortensen et al. (2009) speculated that the slope failure at the western flank of Santo Antão (Fig. 1b) may have been a terminal event of the CG I eruption. They assumed that the CG I eruption is older than the post-collapse Tope de Coroa volcano that was dated by a single analysis to 170±20 ka (Plesner et al., 2002). Our dating reveals that CG I, CG II and FT are much younger than this 170 ka age, i.e. they are considerably younger than at least some older part of the Tope de Coroa volcano, and thus much younger than the western collapse event. Only the CT is old enough (220 ka) for a possible association with the flank collapse but there is no geologic evidence for this. The field evidence that Tope de Coroa eruption products overlie ~107 ka old CG II (Fig. 3a) demonstrates that both CGF and Tope de Coroa volcanic systems coexisted through a significant period of time.

The ages of the CGF also confirm the co-existence of evolved magmas from both magmatic suites (COVA and COROA) on Santo Antão as described by Holm et al. (2006) (Fig. 5). It was the older, basanitic COVA suite that first produced voluminous phonolite erupted as CT about 220 kyrs ago. Following a long period of quiescence until about 106 ka, the younger, nephelinitic COROA system discharged the CG I phonolite, almost immediately followed by the COVA system erupting CG II phonolite. Since the time break between CG I and CG II was too short to be recognized geologically or by radiometric dating, the petrogenetic processes leading to phonolite differentiation must have operated simultaneously in both systems. The subsequent period of time allowed for emplacement of Tope de Coroa scoria layers atop CG II, as well as emplacement of local scoria cone deposits at the Furninha Laie riverbed, before this scoria deposition was interrupted by three fallouts of the FT. This FT magma formed as another product of the COROA system, but less evolved than CG I. From this system also the MF dome extruded some time after CG II emplacement. The precise stratigraphic position of the Aranha Perna dome, which belongs to the COVA system, is still unclear. However, as it is overlain by the CG I tephra, it is clearly older than this event. These alternating eruptions from both magmatic systems document that they both operated simultaneously in the same region of western Santo Antão, and both had evolved to petrologic conditions favoring phonolite generation.

As both magmatic suites generated at least two explosive eruption phases it is of interest if these second eruption phases represent recharge events of the magmatic system or the reanimations of the existing system. At other volcanic systems, the estimated durations of differentiation from mafic to phonolitic compositions average at about 10^5 years (Reagan et al., 1992; Widom et al., 1992; Bourdon et al., 1994; Thomas, 1998; Hawkesworth et al., 2000) whereas differentiation from less evolved phonolite to more evolved phonolite appears to last 100-200 years (Reagan et al, 1992; Condomines et al. 1995; Thomas, 1998; Zellmer et al., 1999). While these time scales vary with reservoir volume and cooling rates as well as

possible replenishments from depth, the time break of nearly 110 ka between CT and CG II (both from the basanite – phonolite COVA suite system; Fig. 5) and the fact that CG II phonolite is less evolved than that of CT (Figs. 4, 5) strongly suggest that CG II represents an entirely independent differentiation event although from similar parental composition as CT. However, CT and CG II demonstrate that repose times of ~100 kyrs in between eruptions need to be considered for Santo Antão.

Although CG I and FT both derived from the COROA suite (Fig. 5), these phonolites differ compositionally (e.g. by their alkali contents; Fig. 4) in a way that cannot be explained by fractional crystallization. While we will investigate petrogenetic processes elsewhere, we here conclude that FT (and the MF lava) formed as a new magma batch independent of previously formed CG I magma.

Although the phonolitic CGF tephras evolved from two compositionally distinct magma systems (Figs. 4, 5), there are some common patterns in behavior. Both suites produced two explosive phonolitic eruptions, each with a stronger first eruption (CT and CG I) indicated by their greater thicknesses (CT and CG I) and wider distribution (CG I), and a weaker second eruption (CG II and FT). The geochemical compositions of the respective second eruptions (CG II and FT) are less evolved compared to the first eruptions (CT and CG I) (Figs. 4, 5). Therefore it would be plausible to explain the weaker second eruptions by lower dissolved gas concentrations in the melt.

Although we cannot presently quantify the age of the FT, and petrogenetic links between the CGF units will be investigated elsewhere, we here conclude that the magma systems forming the four CGF tephras evolved independently from freshly filled reservoirs. The large explosive phonolitic eruptions on Santo Antão thus appear to occur in a stochastic rather than periodic fashion, involving intervals of up to ~100 kyrs, so that forecasting of future events is difficult at best.

9. Conclusions

Our detailed stratigraphic and lithological study of the Cão Grande Formation on Santo Antão identified two new phonolitic tephra units (CT, FT) complementing the two previously recognized (CG I and II). Our new $^{40}Ar/^{39}Ar$ datings reveal a long time gap between the 220 ka CT eruption and the eruptions of CG I and CG II, which occurred in rapid succession at around 106 ka. The age of the younger FT is still unknown. The CGF tephras alternatingly originated from two coexisting magmatic systems (basanitic COVA and nephelinitic COROA system) that both produced two highly explosive eruptions, with a stronger first eruption and a weaker second eruption; evolved dome-forming lavas also leaked from the two systems. The tephra units from both magmatic systems show similar eruption evolutions from stable initial conditions to more unstable conditions, a pattern that may be typical also for future evolved explosive eruptions on the western plateau of Santo Antão.

The CGF age data show that the Tope de Coroa volcano, which grew on top of the western flank collapse scar of Santo Antão, evolved partly contemporaneously with the CGF, having produced 170 ka old rocks as well as deposits covering the 107 ka CG II tephra. A genetic relation between CG I or CG II eruptions and the flank collapse, as previously proposed, can thus be ruled out.

Correlations with marine tephras provide distal dispersal data for the CG I eruption that support a tephra volume of ~10 km^3, about twice the previously published estimate. The CG II tephra volume is ~3 km^3; CT and FT are too scarcely exposed for volume estimates. We also identified ash beds of at least two older, non-CGF phonolitic eruptions in the marine cores. In principle, the CGF ash layers with their unique geochemical glass compositions and wide dispersal form excellent stratigraphic marker horizons in the marine sediment record around the northern Cape Verde Archipelago. However, reworking of primary fallout ash layers - probably favored by the steep submarine flanks of the islands - has led to a

multiplicity of ash layers within distances <150 km from the islands, which are difficult to distinguish from primary layers and may lead to miscorrelations. Based on these observations, we therefore urge extra caution in the identification of primary ash layers during future marine tephrostratigraphic studies.

Acknowledgements

This project was funded by the German Research Foundation (DFG) under grant Fr947/14-1. Many thanks to all members of the scientific party of the METEOR M80/3 expedition for coring, logging, sampling and sample preparation. We thank M. Thöner (GEOMAR) for the great support at the EMP laboratory of GEOMAR, S. Jung (Hamburg University) for providing XRF geochemical analyses and J. Schindlbeck for stimulating discussions. We also appreciate the helpful comments and suggestions of Simon Day and an anonymous reviewer. R. Ramalho acknowledges funding from a FP7-PEOPLE-2011-IOF Marie Curie International Outgoing Fellowship.

References

Ancochea, E., Huertas, M., Hernán, F. and Brändle, J., 2010. Volcanic evolution of Sâo Vicente, Cape Verde Islands: The Praia Grande landslide. J. Volcanol. Geotherm. Res., 198(1): 143-157.

Bebiano, J.B., 1932. A geologia do arquipélago de Cabo Verde. Comun. Serv. de Geol. Portugal 18: 226 pp.

Bourdon, B., Zindler, A. and Wörner, G., 1994. Evolution of the Laacher See magma chamber: Evidence from SIMS and TIMS measurements of U-Th disequilibria in minerals and glasses. Earth Planet. Sci. Lett., 126(1): 75-90.

Burke, K., Wilson, J., 1972. Is the African Plate stationary? Nature 239 (5372): 387–390.

Carey, S., 1997. Influence of convective sedimentation on the formation of widespread tephra fall layers in the deep sea. Geology, 25(9): 839-842.

Carr, M.J., 2000. IGPET for Windows. Somerset, New Jersey, Terra Softa Inc., 52 p.

Condomines, M., Tanguy, J.-C. and Michaud, V., 1995. Magma dynamics at Mt Etna: constraints from U-Th-Ra-Pb radioactive disequilibria and Sr isotopes in historical lavas. Earth Planet. Sci. Lett., 132(1): 25-41.

Dalrymple, G.B., Alexander, E.C., Lanphere, M.A. and Kraker, G.P., 1981. Irradiation of samples for $^{40}Ar/^{39}Ar$ dating using the Geological Survey TRIGA Reactor. U.S. Geological Survey Professional Paper, 1176: 55 pp.

Duprat, H.I., Friis, J., Holm, P.M., Grandvuinet, T. and Sørensen, R.V., 2007. The volcanic and geochemical development of São Nicolau, Cape Verde Islands: Constraints from field and $^{40}Ar/^{39}Ar$ evidence. J. Volcanol. Geotherm. Res., 162(1): 1-19.

Eisma, D. and Passchier, C.A., 1978. Rates of sedimentation on the Cape Verde Rise. Netherlands Journal of Sea Research, 12(1): 107-114.

Fierstein, J. and Nathenson, M., 1992. Another look at the calculation of fallout tephra volumes. Bull. Volcanol., 54: 156-167.

Gerlach, D. C., Cliff, R. A., Davies, G. R., Norry, M., Hodgson, N. (1988). Magma sources of the Cape Verdes archipelago: isotopic and trace element constraints. Geochimica et Cosmochimica Acta, 52(12): 2979-2992.

Graf, H.F., Herzog, M., Oberhuber, J.M. and Textor, C., 1999. Effect of environmental conditions on volcanic plume rise. J. Geophys. Res.: Atmospheres, 104(D20): 24309-24320.

Grevemeyer, I., 1999. Isostatic geoid anomalies over mid-plate swells in the Central North Atlantic. J. Geodyn., 28(1): 41-50.

Günther, D., Jackson, S.E. and Longerich, H.P., 1999. Laser ablation and arc/spark solid sample introduction into inductively coupled plasma mass spectrometers. Spectrochimica Acta Part B: Atomic Spectroscopy, 54(3): 381-409.

Hansteen, T., Kwasnitschka, T. and Klügel, A., 2014. Cape Verde Seamounts - Cruise No. M80/3 - December 29, 2009 - February 1, 2010 - Dakar (Senegal) - Las Palmas de Gran Canaria (Spain). METEOR-Berichte, M80/3: 42 pp.

Hawkesworth, C.J., Blake, S., Evans, P., Hughes, R., Macdonald, R., Thomas, L.E., Turner, S.P. and Zellmer, G., 2000. Time scales of crystal fractionation in magma chambers – integrating physical, isotopic and geochemical perspectives. J. Petrol., 41: 991-1006.

Herzog, M., Graf, H., Textor, C. and Oberhuber, J., 1998. The effect of phase changes of water on the development of volcanic plumes. J. Volcanol. Geotherm. Res., 87: 55-74.

Holm, P.M., Grandvuinet, T., Friis, J., Wilson, J.R., Barker, A.K. and Plesner, S., 2008. An ^{40}Ar-^{39}Ar study of the Cape Verde hot spot: Temporal evolution in a semistationary plate environment. J. Geophys. Res.: Solid Earth, 113(B8): B08201.

Holm, P.M., Wilson, J.R., Christensen, B.P., Hansen, L., Hansen, S.L., Hein, K.M., Mortensen, A.K., Pedersen, R., Plesner, S. and Runge, M.K., 2006. Sampling the Cape Verde mantle plume: Evolution of melt compositions on Santo Antão, Cape Verde Islands. J. Petrol., 47(1): 145-189.

Jørgensen, J.Ø. and Holm, P.M., 2002. Temporal variation and carbonatite contamination in primitive ocean island volcanics from São Vicente, Cape Verde Islands. Chem. Geol., 192(3): 249-267.

Koyaguchi, T. and Woods, A.W., 1996. On the formation of eruption columns following explosive mixing of magma and surface-water. J. Geophys. Res., 101: 5561-5574.

Kutterolf, S., Freundt, A. and Burkert, C., 2011. Eruptive history and magmatic evolution of the 1.9 kyr Plinian dacitic Chiltepe Tephra from Apoyeque volcano in west-central Nicaragua. Bull. Volcanol., 73(7): 811-831.

Kutterolf, S., Freundt, A. and Peréz, W., 2008. The Pacific offshore record of Plinian arc volcanism in Central America, part 2: Tephra volumes and erupted masses. Geochem. Geophys. Geosys., 9(2): doi:10.1029/2007GC001791.

Le Maitre, R.W., Bateman, P., Dudek, A., Keller, J., Lameyre, J., Le, B.a.s., Sabine, P.A., Schmid, R., Sorensen, H., Streckeisen, A., Woolley, A.R. and Zanettin, B., 1989. A classification of igneous rocks and glossary of terms. Blackwell Scientific Publ., Oxford - London - Edinburgh - Boston - Melbourne, 193 pp.

McNutt, M., 1988. Thermal and mechanical properties of the Cape Verde Rise. J. Geophys. Res.: Solid Earth, 93(B4): 2784-2794.

Mitchell, J.G., Le Bas, M.J., Zielonka, J. and Furnes, H., 1983. On dating the magmatism of Maio, Cape Verde Islands. Earth Planet. Sci. Lett., 64(1): 61-76.

Montelli, R., Nolet, G., Dahlen, F., Masters, G., Engdahl, E.R. and Hung, S.-H., 2004. Finite-frequency tomography reveals a variety of plumes in the mantle. Science, 303(5656): 338-343.

Mortensen, A.K., Wilson, J.R. and Holm, P.M., 2009. The Cão Grande phonolitic fall deposit on Santo Antão, Cape Verde Islands. J. Volcanol. Geotherm. Res., 179(1-2): 120-132.

NOAA-CIRES, 2001. Data provided from NCEP climate diagnostics center, Boulder, Colorado: http://www.cdc.noaa.gov/cgi-bin/DataMenus.pl?dataset=NCEP

Norman, M., Pearson, N., Sharma, A. and Griffin, W., 1996. Quantitative analysis of trace elements in geological materials by laser ablation ICPMS: instrumental operating conditions and calibration values of NIST glasses. Geostandards Newsletter, 20(2): 247-261.

Phipps Morgan, J., Morgan, W.J. and Price, E., 1995. Hotspot melting generates both hotspot volcanism and a hotspot swell? J. Geophys. Res.: Solid Earth, 100(B5): 8045-8062.

Plesner, S., Holm, P.M. and Wilson, J.R., 2002. ^{40}Ar-^{39}Ar geochronology of Santo Antão, Cape Verde islands. J. Volcanol. Geotherm. Res., 120: 103-121.

Pyle, D.M., 1989. The thickness, volume and grain size of tephra fall deposits. Bull. Volcanol., 51: 1-15.

Ramalho, R., Helffrich, G., Cosca, M., Vance, D., Hoffmann, D., Schmidt, D. N., 2010a. Episodic swell growth inferred from variable uplift of the Cape Verde hotspot islands. Nature Geoscience, 3(11): 774-777.

Ramalho, R., Helffrich, G., Schmidt, D. and Vance, D., 2010b. Tracers of uplift and subsidence in the Cape Verde archipelago. J. Geol. Soc. London, 167(3): 519-538.

Reagan, M.K., Volpe, A.M. and Cashman, K.V., 1992. ^{238}U- and ^{232}Th-series chronology of phonolite fractionation at Mount Erebus, Antarctica. Geochim. Cosmochim. Acta, 56(3): 1401-1407.

Renne, P.R., Swisher, C.C., Deino, A.L., Karner, D.B., Owens, T.L. and DePaolo, D.J., 1998. Intercalibration of standards, absolute ages and uncertainties in ^{40}Ar/^{39}Ar dating. Chem. Geol., 145(1): 117-152.

Sandwell, D.T., Müller, R.D., Smith, W.H., Garcia, E. and Francis, R., 2014. New global marine gravity model from CryoSat-2 and Jason-1 reveals buried tectonic structure. Science, 346(6205): 65-67.

Stillman, C., Furnes, H., LeBas, M., Robertson, A. and Zielonka, J., 1982. The geological history of Maio, Cape Verde islands. J. Geol. Soc. London, 139(3): 347-361.

Tarff, R. and Day, S., 2013. Chilled margin fragmentation as a trigger for transition from Strombolian to phreatomagmatic explosive activity at Cova de Paul Crater, Santo Antão, Cape Verde Islands. Bull. Volcanol., 75(7): 1-14.

Thomas, L.E., 1998. Uranium series, major and trace element geochemistry of lavas from Tenerife and Lanzarote, Canary Islands, PhD thesis, Open University, London, UK: 247 pp..

Torres, P., Silva, L., Serralheiro, A., Tassinari, C. and Munhá, L., 2002. Enquadramento geocronológico pelo método K/Ar das principais sequências vulcano-estratigráficas da Ilha do Sal - Cabo Verde. Garcia de Orta, 18: 9-13.

Valentine, G. and Fisher, R., 2000. Pyroclastic surges and blasts. In: Sigurdsson, H., et al., eds., Encyclopedia of Volcanoes, Academic Press: 571-580.

Van Achterbergh, E., Ryan, C., Jackson, S.E., Griffin, W.L., 2001. Data reduction software for LA-ICPMS. In: P. Sylvester (Ed.), Laser Ablation-ICPMS in the Earth Sciences. Mineralogical Association of Canada Short course handbook: pp. 239‑243.

Widom, E., Schmincke, H.-U. and Gill, J., 1992. Processes and timescales in the evolution of a chemically zoned trachyte: Fogo A, Sao Miguel, Azores. Contrib. Mineral. Petrol., 111(3): 311-328.

Woods, A.W., 1988. The fluid dynamics and thermodynamics of eruption columns. Bull. Volcanol., 50: 169-193.

Zellmer, G.F., Blake, S., Vance, D., Hawkesworth, C. and Turner, S., 1999. Plagioclase residence times at two island arc volcanoes (Kameni Islands, Santorini, and Soufriere,

St. Vincent) determined by Sr diffusion systematics. Contrib. Mineral. Petrol., 136(4): 345-357.

Zhang, R., Jahn, B., Liou, J., Yang, J., Chiu, H., Chung, S., Li, T. and Lo, C., 2010. Origin and tectonic implication of an UHP metamorphic mafic and ultramafic complex from the Sulu UHP terrane, eastern China: Evidence from petrological and geochemical studies of CCSD-Main Hole core samples. Chem. Geol., 276(1): 69-87.

Figure captions

Figure 1: a) Overview map of the Cape Verde Archipelago with bathymetric data from Sandwell et al. (2014). M80/3 gravity core stations (red dots) and schematic profiles of cores used in this study are shown. The red rectangle marks the main study area on Santo Antão. ODP and DSDP core stations (yellow dots) are shown for comparison. **b)** Satellite map of the western plateau on Santo Antão (map source Google Earth). Red dots mark type localities and black dots mark additional outcrops logged for this study. Phonolitic domes are marked by black dotted lines. Blue lines are riverbeds mentioned in this study. Red dotted line traces slope failure scarp partly covered by Tope de Coroa volcano.

Figure 2: Composite stratigraphic succession of the Cão Grande Formation combining the four type localities on the western plateau of Santo Antão. CT is marked in red, CG I in blue, CG II in green and FT in purple, fluvially reworked debris horizons are marked with RW. Scale represents the maximum thickness for each unit. The interval of re-interpreted beds at the transition from CG I to CG II - discussed in the text - is marked with an asterisk (*).

Figure 3: a) Type locality of CT in the Ribeira de Canudo, CT and CG I are separated by reworked debris (RW), whereas CG II concordantly overlies CG I. Red dashed lines mark unit boundaries. For scale the CG I deposit is about 8 m thick in this outcrop. **b)** Transition from pumice to scoria clasts within FT-A3. Subunit boundary is marked by red dashed line. Scraper for scale is 30 cm long. **c)** Proximal outcrop in the Ribeira de Canudo showing the phreatomagmatic deposits of the top of CG I and base of CG II. The top of CG I is discordantly cut (red dashed line) by CG II surges. This is the interval marked by * in Fig. 2.

The scale is 2 m long. **d)** Type locality of CG I in the Cão Grande riverbed. CG I is 8.25 m thick at this outcrop and is concordantly overlain by CG II.

Figure 4: Whole-rock total alkalis versus silica classification diagram (Le Maitre et al., 1989) for rocks from the CGF and the domes of Morro de Figueira (cross) and Monte Aranha Perna (asterisk). Additional volcanic rock compositions from Santo Antão (light gray squares) from Holm et al. (2006) are shown for comparison.

Figure 5: Whole-rock Zr vs. Rb variation diagram with trends after Holm et al. (2006). CT, CG II and the Monte Aranha Perna (AP) rocks are associated to the basanite – phonolite trend (COVA), whereas CG I, FT and Morro de Figueira (MF) are following the nephelinite – phonolite trend (COROA). Volcanic rock compositions (light gray squares) from Holm et al. (2006) are shown.

Figure 6: Phenocryst contents vs. stratigraphic height. Volume percentages refer to vesicle-free compositions. Calculated phenocryst contents are marked by filled symbols, visually estimated contents by open symbols.

Figure 7: Schematic profiles of M80/3 gravity cores (cf. Fig. 1a). Beds containing ash correlated to the CGF are labeled in blue (CG I) and green (CG II), non-CGF phonolitic ash layers in light brown and mafic ash layers in black. Triangles mark CG II ash beds with homogeneous glass-shard compositions. Blue lines indicate correlations between the CG I ash beds. The expected position of the primary CG I and CG II ash layers relative to the cores are indicated by arrows.

Figure 8: Matrix-glass compositions of felsic marine ash layers from cruise M80/3 (normalized to anhydrous composition) compared with glass-composition fields of tephras from the CGF. Marine data are averages of all analyses made for each ash layer (see supplement for detailed glass-analytical data). Additional phonolitic rock compositions from

the Proto Coroa unit and the Cova unit from Santo Antão after Holm et al. (2006) are shown for comparison. Note that sample numbers begin with core number followed by depth (interval) below seafloor (in cm) of the ash bed. Gray bars show 2σ standard deviation for each sample, samples without gray bars have standard deviations smaller than symbol size.

Figure 9: A: Isopach map for the CG I tephra with on land isopachs of CG I taken from Mortensen et al. (2009). B: Isopach map of CG II calculated by summing up ash beds in each core, for details see text. Dashed lines indicate that offshore isopachs are constrained by few available data only. **Bold** numbers mark cores used to construct isopachs, *italic* numbers mark thicknesses.

Appendices

A: Core descriptions

B: CG EMP-Data

CG LA-ICPMS-Data

Marine glass-EMP-Data

Marine glass-LA-ICPMS-Data

Ar-Ar-Data

Crystallinity calculations

GPS-coordinates for outcrop locations

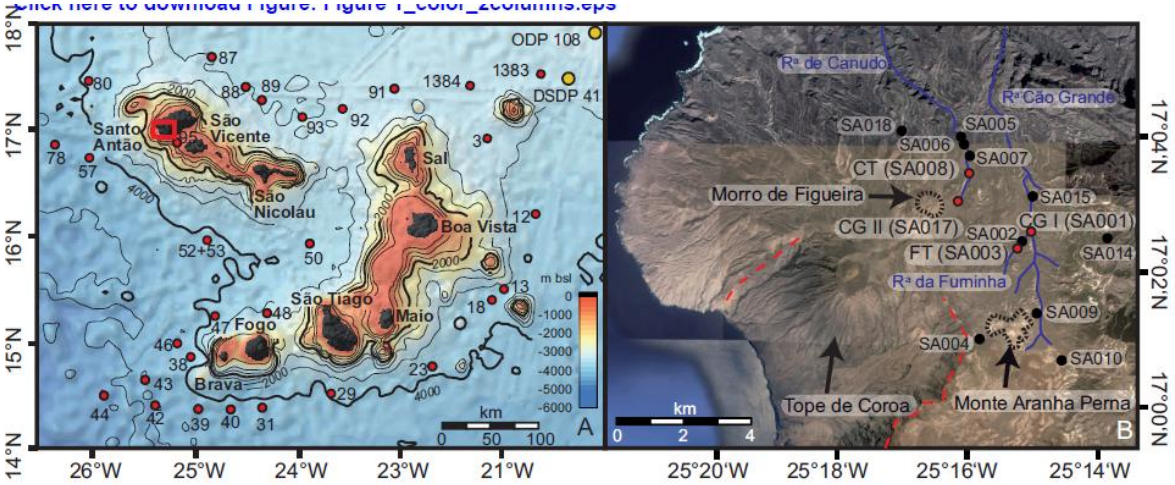

Figure 1

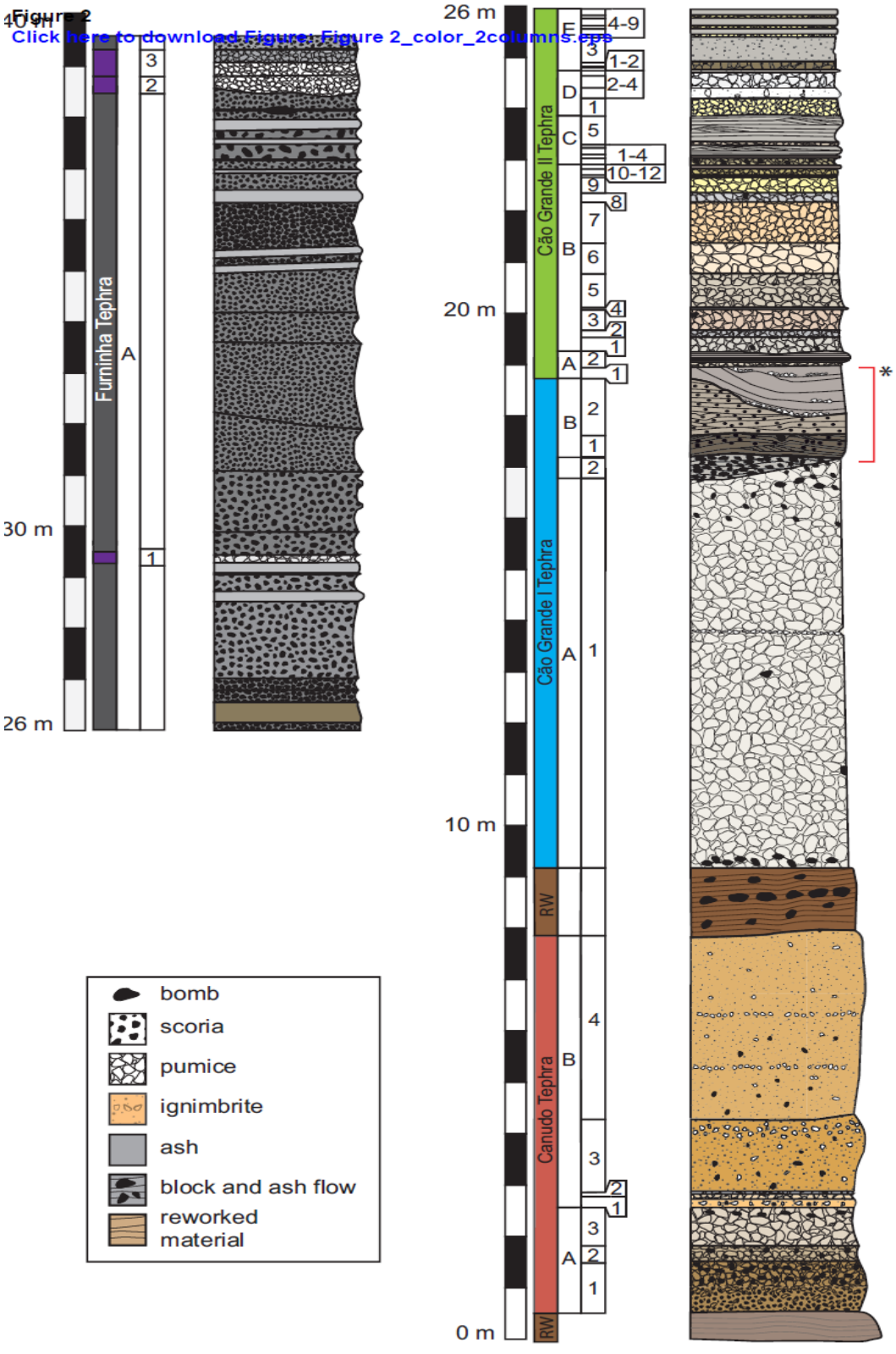

Figure 2

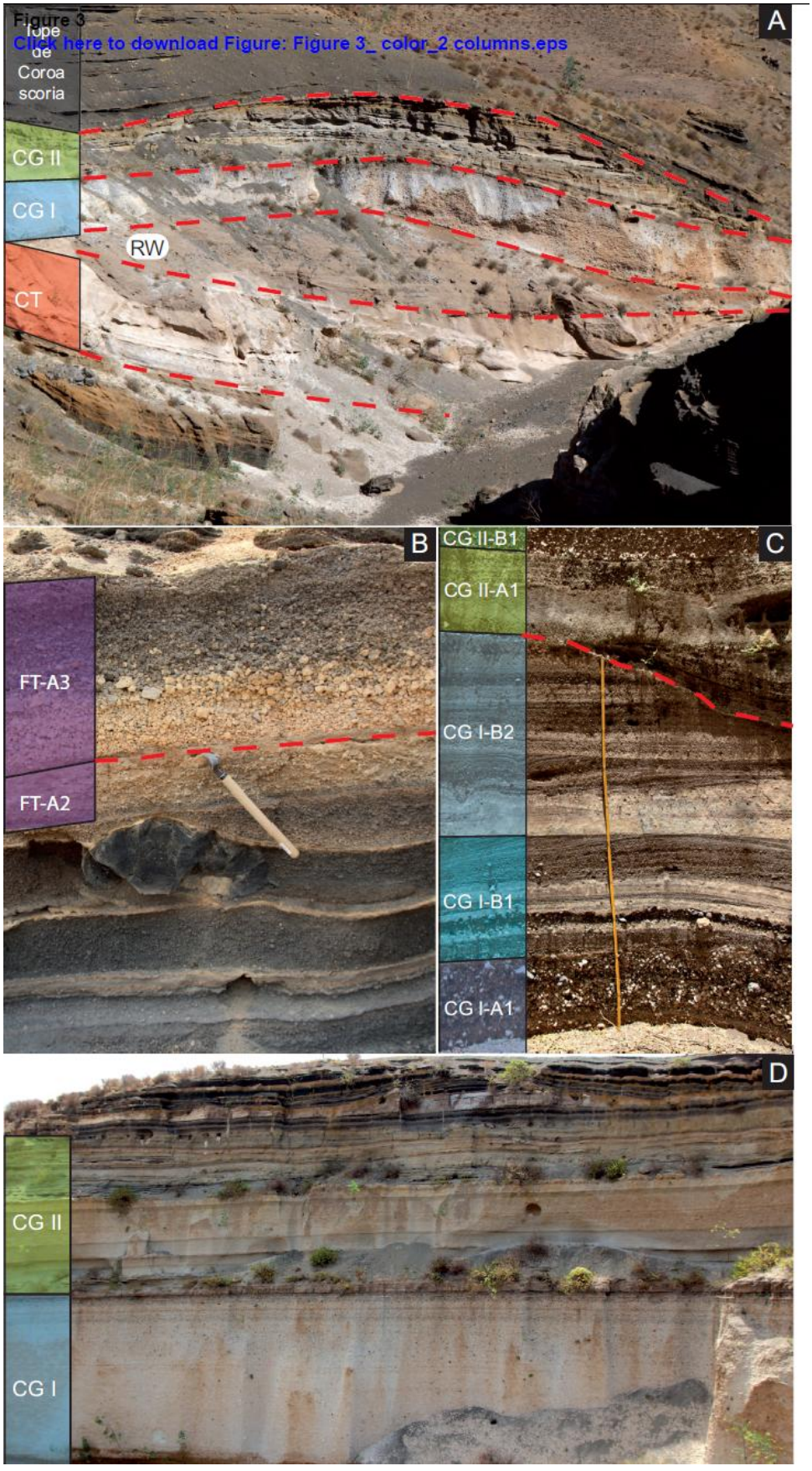
Figure 3
Click here to download Figure: Figure 3_ color_2 columns.eps
A
Tope de Coroa scoria
CG II
CG I
RW
CT
B
FT-A3
FT-A2
C
CG II-B1
CG II-A1
CG I-B2
CG I-B1
CG I-A1
D
CG II
CG I

Figure 3

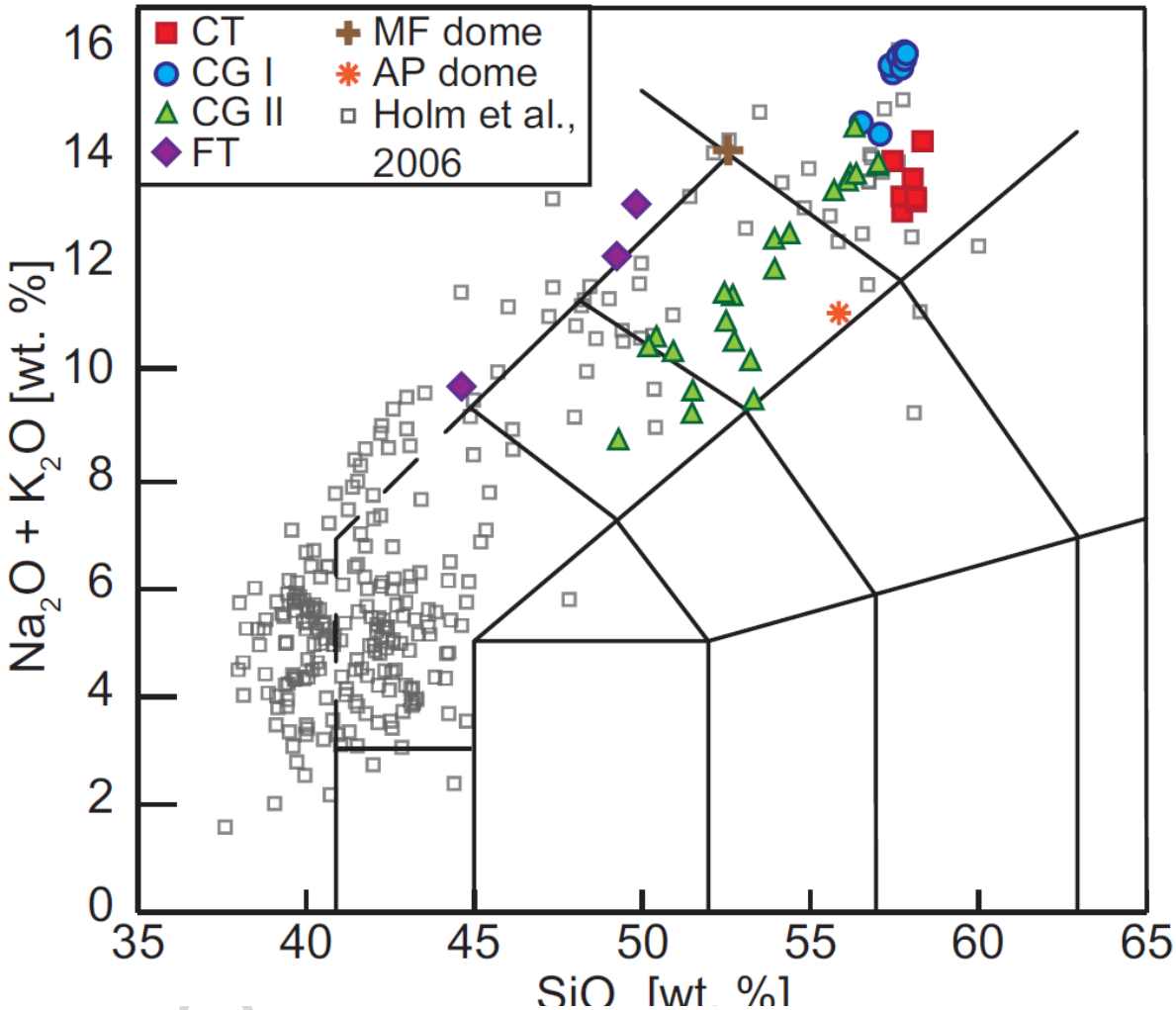

Figure 4

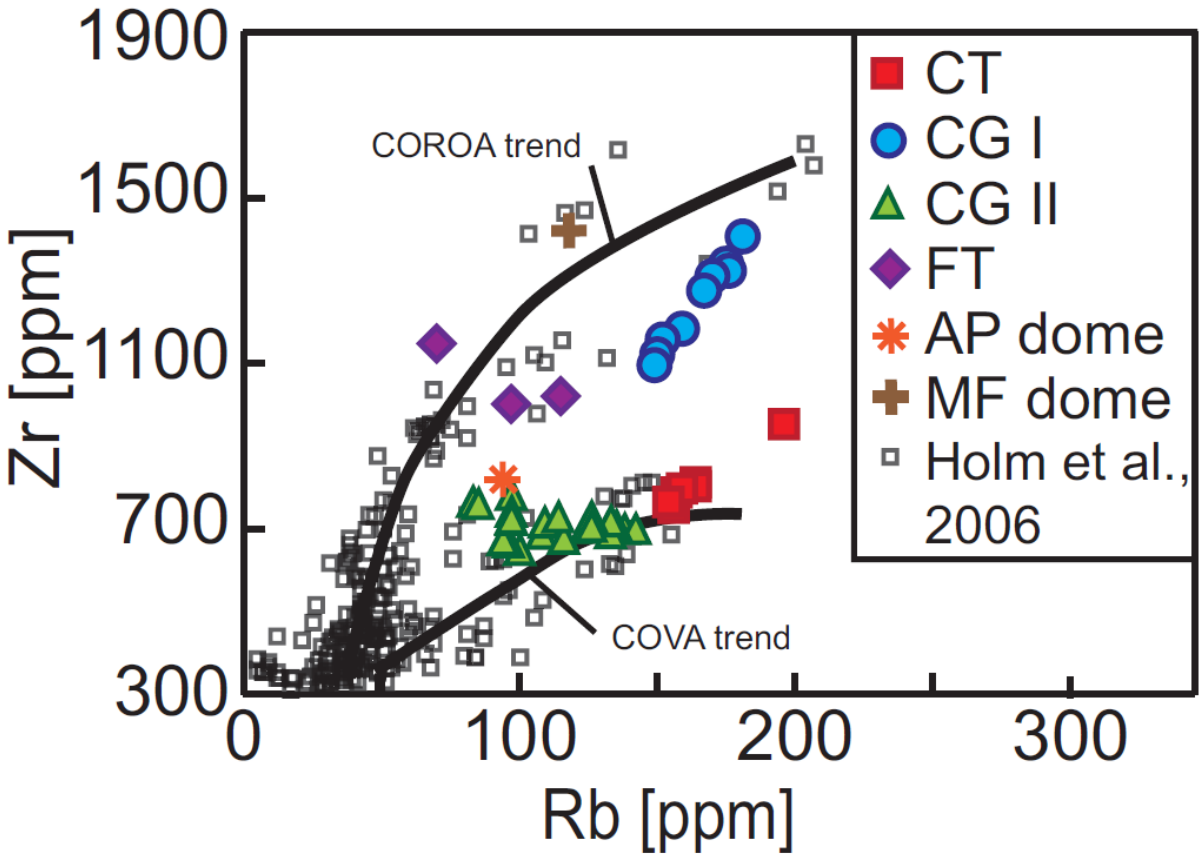

Figure 5

Figure 6
Click here to download Figure: Figure 6_color_1column.eps

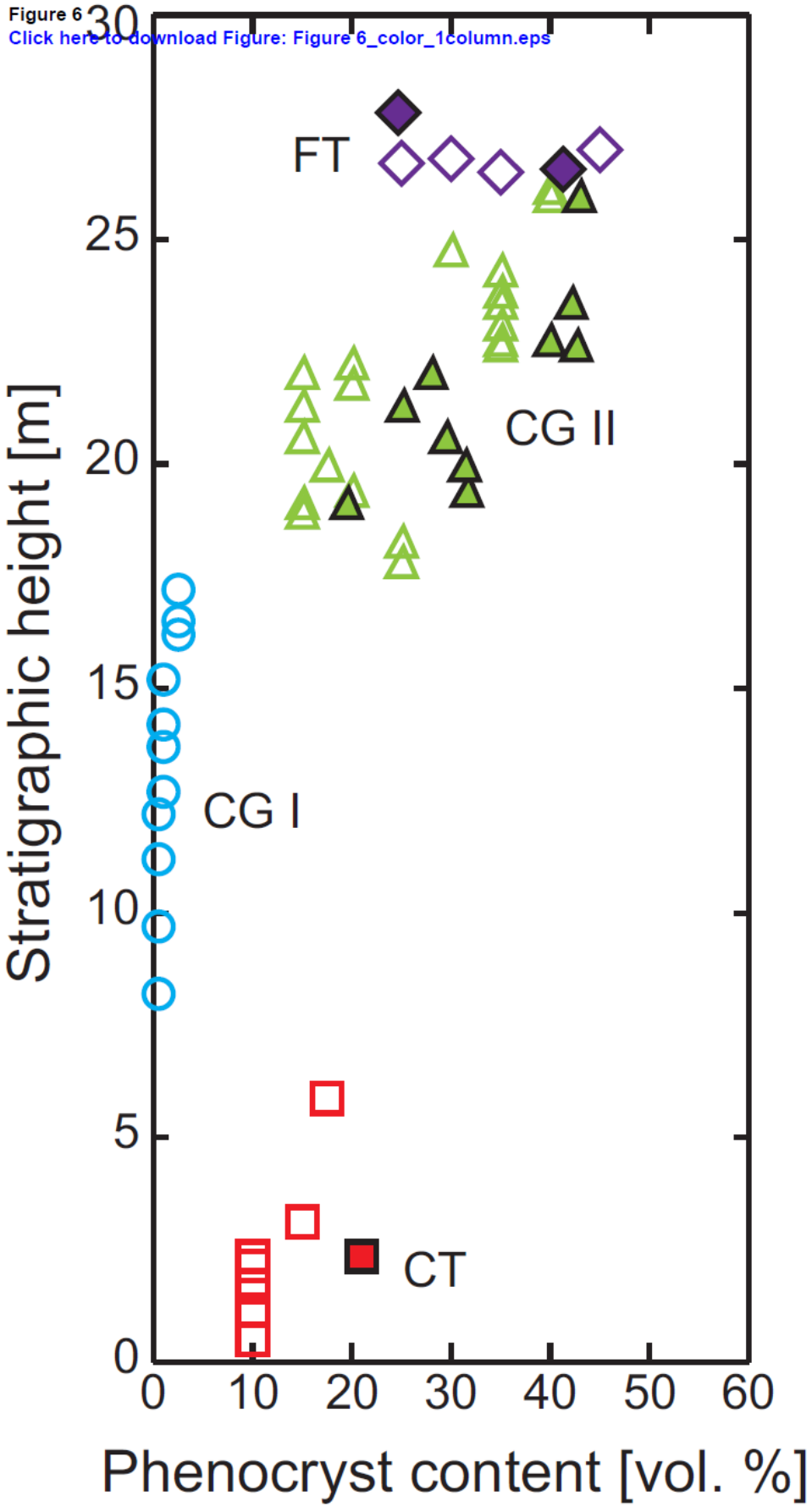

Figure 6

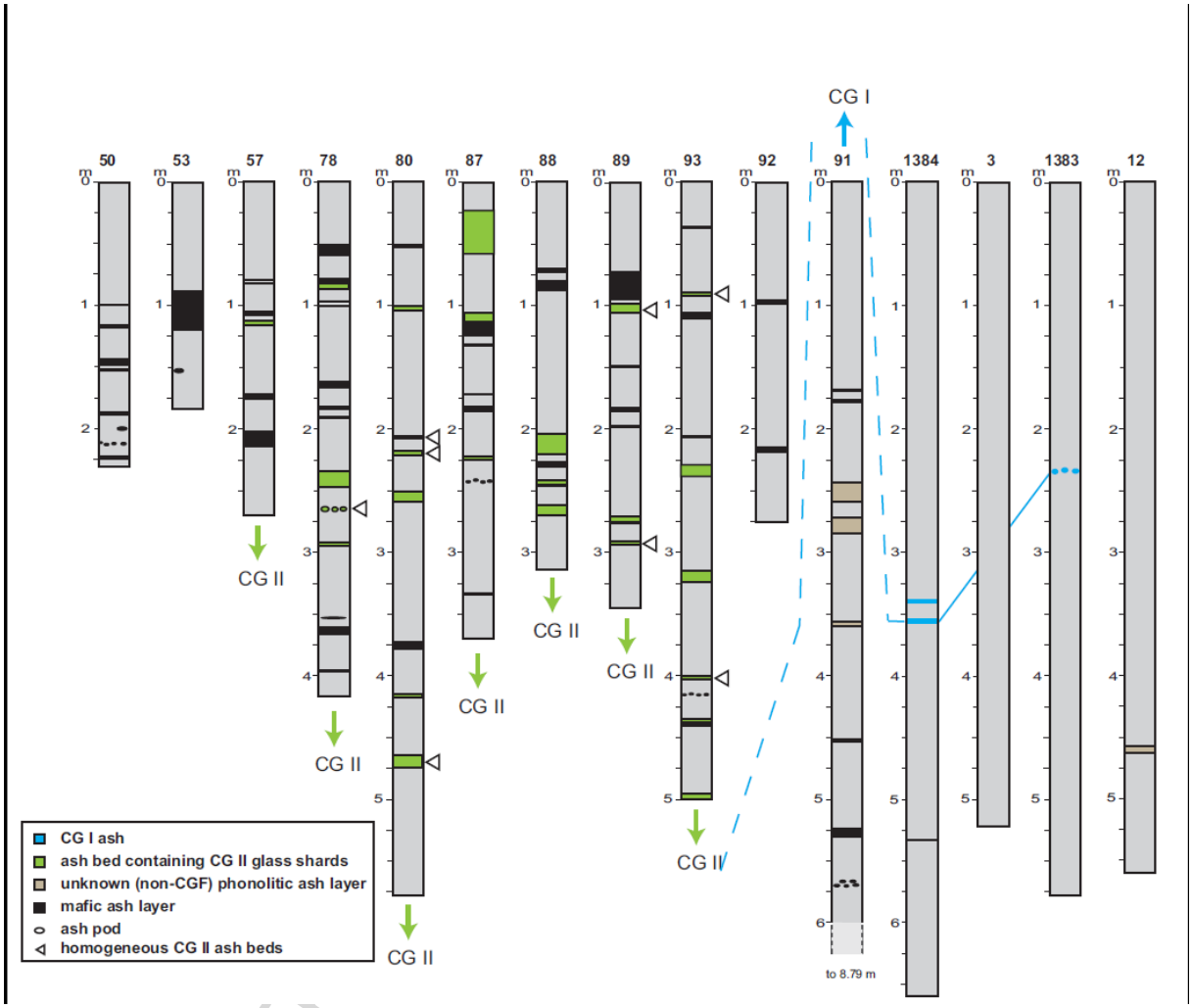

Figure 7

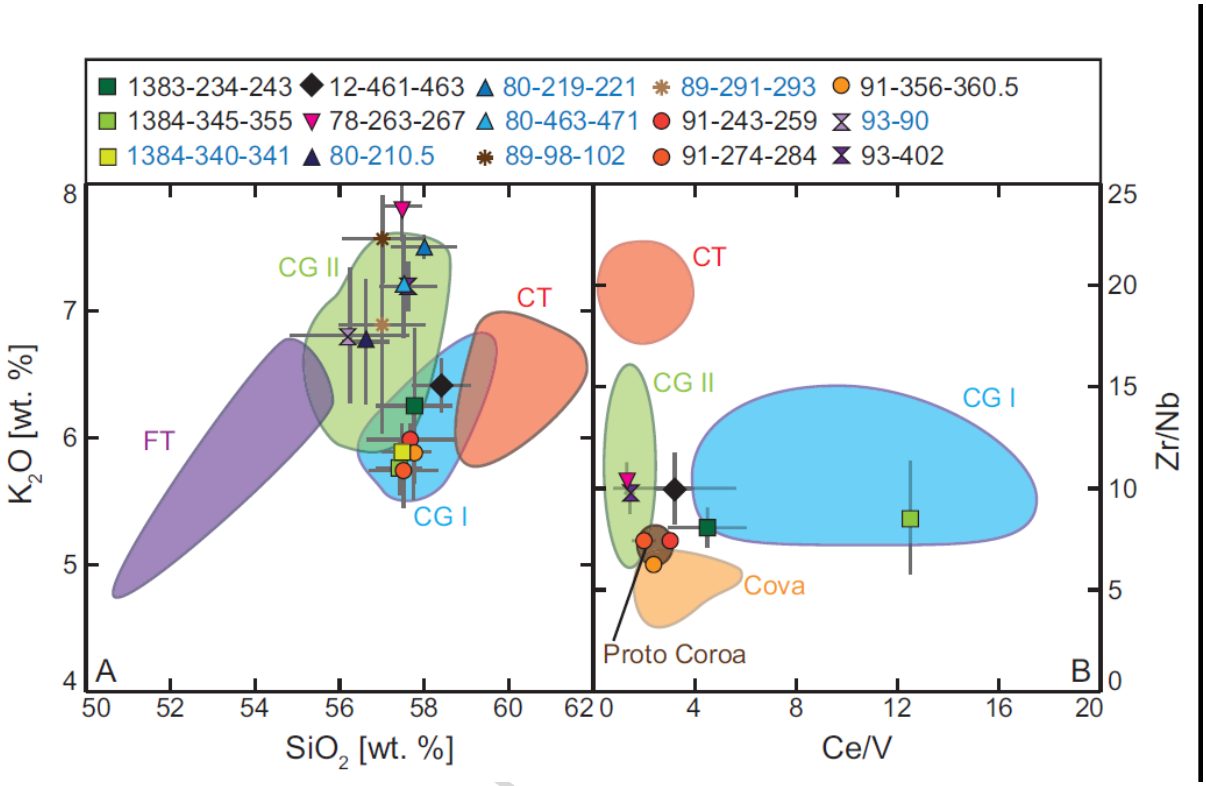

Figure 8

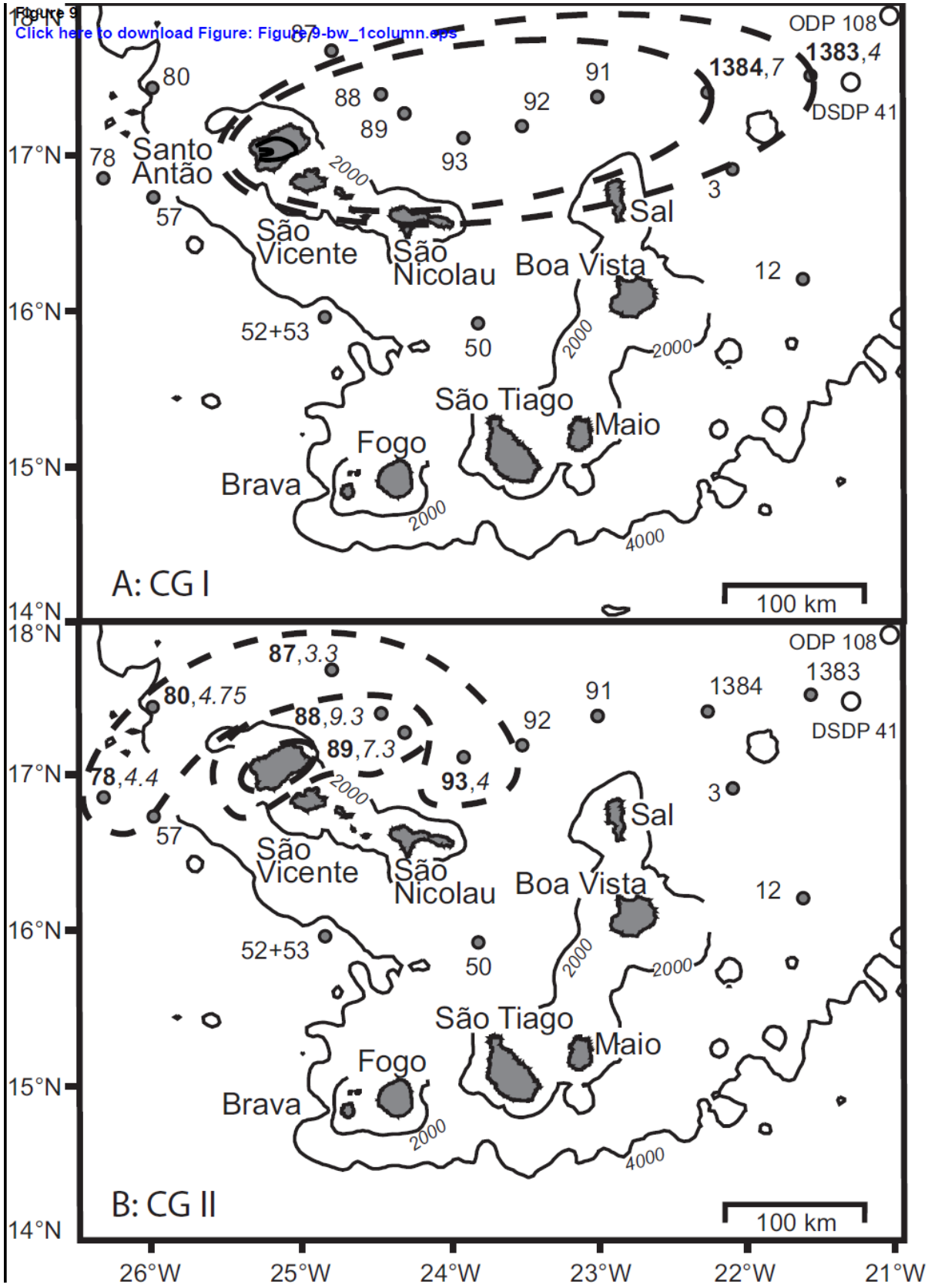

Figure 9